Catena 222 (2023) 106866

Contents lists available at ScienceDirect

Catena

journal homepage: www.elsevier.com/locate/catena

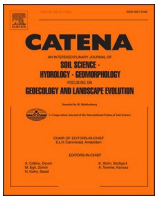

Landslide susceptibility mapping and dynamic response along the Sichuan-Tibet transportation corridor using deep learning algorithms

Wubiao Huang [a,b], Mingtao Ding [a,b,c,*], Zhenhong Li [a,b,c,*], Junchuan Yu [d], Daqing Ge [d], Qi Liu [a,b], Jing Yang [a,b]

[a] College of Geological Engineering and Geomatics, Chang'an University, Xi'an 710054, China
[b] Big Data Center for Geosciences and Satellites, Chang'an University, Xi'an 710054, China
[c] Key Laboratory of Western China's Mineral Resource and Geological Engineering, Ministry of Education, Xi'an 710054, China
[d] China Aero Geophysical Survey and Remote Sensing Center for Natural Resources, Beijing 10083, China

ARTICLE INFO

Keywords:
Landslide susceptibility mapping
The Sichuan-Tibet transportation corridor
Conv-SE-LSTM
Dynamic response
Robustness

ABSTRACT

Landslides are one of the most serious natural hazards along the Sichuan-Tibet transportation corridor, which crosses the most complicated region in the world in terms of topography and geology. Landslide susceptibility mapping (LSM) is in high demand for risk assessment and disaster reduction in this mountainous region. A new model, namely Convolutional-Squeeze and Excitation-long short-term memory network (Conv-SE-LSTM), is proposed to map landslide susceptibility along the Sichuan-Tibet transportation corridor. Compared with conventional deep learning models, the proposed Conv-SE-LSTM adaptively emphasizes the contributing features of the conditioning factors by Squeeze and Excitation network (SE), and elaborately arranges the input order of the conditioning factors to utilize their dependence by long short-term memory network (LSTM). Considering the complex geological conditions and the wide range of the study area, the generalization and robustness of the proposed model are demonstrated from the perspective of global and sub-regions. Our proposed model yielded the best Area Under Curve (AUC) value of 0.8813, which is about 3%, 4% and 8% higher than that obtained by three traditional methods, respectively. An annual scale landslide susceptibility changes analysis method is also presented with an accuracy rate of 93.33%. The dynamic response relationship between landslide susceptibility and conditioning factors is revealed.

1. Introduction

The Sichuan-Tibet transportation corridor – part of China's integrated transport system – is one of the prime considerations of the Great Western Development Strategy (GWDS), mainly because of its role in promoting transportation, tourism, and economic and social development along its entire course (Guo et al., 2017; Peng et al., 2020). The transportation corridor has an average altitude of 3800 m, and passes through areas with dramatically fluctuating topography, complex geology and strong tectonic movement (Peng et al., 2020). The transportation corridor is frequently affected by geological hazards, of which landslides are the most common and pose the greatest threat to the transportation project and people's lives in the region (Guo et al., 2017). Therefore, landslide susceptibility mapping (LSM) is of great significance for risk assessment and disaster reduction.

LSM involves a comprehensive analysis of various factors, including geological environmental factors, historical landslides and the landslide physical laws of an area, to determine the probability of future landslide events in that area (Li et al., 2017b; Reichenbach et al., 2018). LSM is largely divided into two methods, viz. qualitative and quantitative methods. Qualitative methods rely mainly on expert experience, such as the expert system scoring method and the analytic hierarchy process (AHP, Bathrellos et al., 2017; Lyu et al., 2018; Nefeslioglu et al., 2013). Quantitative methods mainly include the deterministic methods based on physical models, the data-driven methods based on statistical models (Kritikos and Davies, 2014; Li et al., 2017b; Zhang et al., 2020) and the machine learning methods (Di Napoli et al., 2020; Fang et al., 2020; Karakas et al., 2022; Kocaman et al., 2020; Sun et al., 2021; Yu et al., 2019). The common machine learning methods include logistic regression (LR, Aditian et al., 2018; Goyes-Peñafiel and Hernandez-Rojas, 2021), random forest (RF, Rabby et al., 2020; Sun et al., 2020), support vector machine (SVM, Pradhan, 2013; Xu et al., 2012), artificial

* Corresponding authors at: College of Geological Engineering and Geomatics, Chang'an University, Xi'an 710054, China.
E-mail addresses: mingtaoding@chd.edu.cn (M. Ding), zhenhong.li@chd.edu.cn (Z. Li).

https://doi.org/10.1016/j.catena.2022.106866
Received 18 July 2022; Received in revised form 11 November 2022; Accepted 9 December 2022
Available online 22 December 2022

neural network (ANN, Ermini et al., 2005; Lee et al., 2020; Zeng and Chen, 2021), and others.

In recent years, deep learning technology has seen significant application in the fields of image classification (Krizhevsky et al., 2017), change detection (Hou et al., 2021) and landslide detection (Can et al., 2019; Ji et al., 2020; Mohan et al., 2021). The method can deal with non-linear problems well, and some scholars apply it to landslide susceptibility mapping. Wang et al. (2019) first constructed the Convolutional Neural Network (CNN) models for LSM, which automatically learned complicated non-linear mapping from conditioning factors to ground truth through a series of convolutional layers. Yang et al. (2021) proposed a hybrid model based on CNN, which applied two-dimensional CNN to extract landslide spatial information and one-dimensional CNN to obtain the correlation characteristics between the conditioning factors. Wang et al. (2020) proposed a sequential data representation method to explore the prediction potential of Recurrent Neural Network (RNN). The authors reported three RNN models (long short-term memory (LSTM), gated recurrent unit (GRU) and simple recurrent unit (SRU)) for landslide susceptibility evaluation. Wang et al. (2021) proposed an integrated method of stacking CNN and RNN for LSM. CNN was used to extract effective deep features and RNN model was adopted to make use of the sequence information of the data. The integrated method achieved a better performance than an individual CNN or LSTM. Wei et al. (2022) developed an attention-constrained neural network with overall cognition (OC-ACNN) for susceptibility prediction. The overall cognition based on frequency ratio was introduced as the priori information on the hidden layer to yield the effect of attention.

Actually, the occurrence of landslides is affected by both topographic conditions and triggering conditions. In comparision with topographic conditions, triggering conditions have time attributes and always change with time. Therefore, landslide susceptibility also correspondingly dynamically changes (Torizin et al., 2018). Rainfall is one of the main triggering factors of landslides (Jones et al., 2021) and many studies focus on the dynamic changes of susceptibility under dynamic rainfall conditions. Caine (1980) first proposed a relationship between rainfall intensity and duration for landslide prediction. Pradhan et al. (2018) used a risk matrix to evaluate the joint probability of landslides and triggering rainfall threshold which can be applied to areas with incomplete data or non-recurrent landslide events. At the same time, some scholars also discussed the change of landslide susceptibility under integrated dynamic factors. Hua et al. (2020) comprehensively studied the dynamic changes of landslide susceptibility under the factors of rainfall, reservoir water level, and land use change in the Three Gorges Reservoir Area in 2002, 2007 and 2017. Li et al. (2020) adopted two dynamic factors, namely rainfall and human activities, to study the dynamic changes of landslide susceptibility in the Three Gorges Reservoir Area in 2010, 2015 and 2019. Torizin et al. (2018) studied the landslide susceptibility changes in Lanzhou in 2000, 2012 and 2016, and used dynamic factors such as DEM and land use. Due to the coverage of the study area, characteristics of topography and data availability in this research, two dynamic change factors, namely rainfall and NDVI, were selected for research.

Although many issues have been discovered, two of them remain unsolved in deep learning-based LSM: (1) Most of the deep learning methods are successfully applied to moderate study areas, such as cities or counties, with homogeneous geological conditions. However, the performance of the deep learning models needs to be further discussed for study areas with complex geological conditions and wide range. (2) The occurrence of landslides is affected by various conditioning factors, which have different contributions to landslide occurrence. How to take full advantage of the interdependence between the conditioning factors to improve the performance of LSM needs to be further discussed.

The main contributions of this study can be summarized as follows. First, a Convolutional-Squeeze and Excitation-Long short term memory network (Conv-SE-LSTM) model was proposed for LSM. The proposed model adaptively optimized the weights of conditioning factor to enhance the contributing features, and took full advantage of the factor dependence to improve the efficiency. Secondly, the Sichuan-Tibet transportation corridor with complex geological conditions and wide coverage was selected as the study area. The study area was divided into several sub-regions according to the water systems, the geological conditions, the mechanism of landslides and the number of landslides. The robustness and generalization of four deep learning models were compared at different scales in terms of accuracy, precision, recall, F-measure, receiver operating characteristic (ROC) and area under curve (AUC). Finally, an annual scale landslide susceptibility changes analysis method was presented. The Conv-SE-LSTM was employed to predict the susceptibility index under different annual cumulative rainfall (ACR) and normalized difference vegetation index (NDVI) conditions. The dynamic response relationship between landslide susceptibility and dynamic factors was revealed.

2. Study area and data

2.1. Description of the study area

The Sichuan-Tibet transportation corridor commences in Chengdu, Sichuan Province. Before terminating in Lhasa, it passes through Ya'an, Kangding, Changdu, Bomê and Linzhi. The rail route has a total length of 1543 km and crosses seven rivers, namely the Minjiang River, the Dadu River, the Ya-lung River, the Jinsha River, the Lancang River, the Salween River and the Brahmaputra River. It passes through eight mountains, including the Longmen Mountains, the Hengduan Mountains, the Nyainqentanglha Mountains, the Gangdise Mountains and the Himalayas (Peng et al., 2020). The study area covers 1332.5 km of the Sichuan-Tibet transportation corridor from east to west and a width of 427 km from south to north, the area totaling 57×10^4 km^2 (see Fig. 1). It covers the most complex geological, topographical and geomorphic areas in the world (Guo et al., 2017). The average annual temperature and rainfall levels decrease from east to west with increased altitude. The faults in the area are well developed and the lithology mainly comprises granite, sandstone, limestone and loose deposits.

A total of 1669 landslides were identified in this study, of which 1590 landslides had only location information and were used for spatial scale analysis of LSM, while 79 landslide events contained occurrence time information from 2010 to 2018, and were used to verify the accuracy of dynamic change of landslide susceptibility. The 1590 landslide points were obtained from historical landslide records, interpretation of Google Earth images and Interferometric Synthetic Aperture Rader (InSAR) technology, and confirmed through field investigation and by the railway department (China Railway Eryuan Engineering Group Co. ltd). These landslides were identified based on the deformation and morphological information of landslide hazards, which can be divided into three categories (Li et al., 2022): (1) 850 (53.46 %) areas with obvious deformation signs and characteristics are currently undergoing deformation, which are called actively deforming slopes. (2) 179 landslides (11.26 %) that have occurred and are still deformed are called reactivated historically deformed slopes. (3) 561 landslides (35.28 %) that have occurred and are currently in a stable state are called stabilized historically deformed slopes. The 79 landslide events were selected from the Global Landslide Catalog (GLC) which are available free of charge from the National Aeronautics and Space Administration (NASA, https://gpm.nasa.gov/landslides, (Pradhan, 2013; Xu et al., 2012). "Landslides_SL" was used to represent the first-mentioned 1590 landslides and "Landslides_NASA" represented the second-mentioned 79 landslide events. The landslide inventory map of the study area is shown in Fig. 1.

2.2. Landslide conditioning factors

The occurrence of landslides is affected by several factors such as topography, geology, hydrological, land cover and human activity.

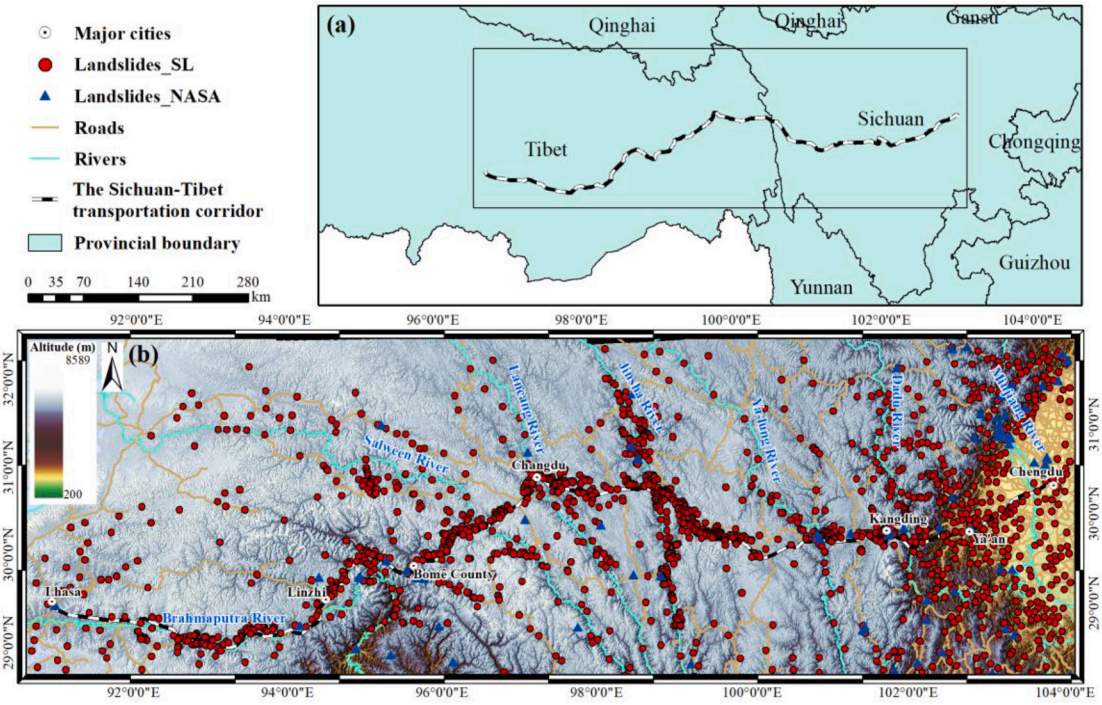

Fig. 1. Landslide inventory mapping along the Sichuan-Tibet transportation corridor. "Landslides_SL" was used to represent the first-mentioned 1590 landslides and "Landslides_NASA" represented the second-mentioned 79 landslide events.

Based on the geological conditions of the study area and previous studies (Li et al., 2017a), 15 conditioning factors were selected for LSM; 13 were static factors (altitude, slope, aspect, curvature, plan curvature, profile curvature, relief amplitude, surface roughness, topographic wetness index (TWI), lithology, distance to roads, distance to rivers and distance to faults) and two were dynamic factors (NDVI and ACR). In mapping spatial susceptibility, the two dynamic factors were replaced using multi-year average cumulative rainfall (MYACR) and NDVI-mean. The data sources of these factors are listed in Table 1 and the thematic maps are shown in Fig. 2. All the landslide conditioning factors were converted into a raster form with a grid size of 30 × 30 m.

Fig. 3 shows the average ACR (i.e., the mean of annual cumulative rainfall in a certain year in the study area) and the number of Landslides_NASA from 2010 to 2018. The landslide events in the study area have been recorded only up to 2018. The largest number of landslide events occurred in 2011 which was 20, followed by 2010, 2012, 2016 and 2018. The average ACR was the lowest in 2011. According to the largest number of landslide events and the largest change in the average ACR, the five-year timespan from 2011 to 2016 was finally selected to analyze the change in the susceptibility index.

Table 1
Datasets used in this study.

Data	Source	Data	Source
Landsat8 OLI imagery	https://www.gscloud.cn	Slope	30 m SRTM DEM
30 m SRTM DEM	https://gdex.cr.usgs.gov/gdex/	Aspect	30 m SRTM DEM
Lithology	https://geocloud.cgs.gov.cn	Curvature	30 m SRTM DEM
Roads	https://www.webmap.cn	Plan curvature	30 m SRTM DEM
Faults	https://geocloud.cgs.gov.cn	Profile curvature	30 m SRTM DEM
Rivers	https://www.webmap.cn	Surface roughness	30 m SRTM DEM
ACR	https://gpm.nasa.gov/	Relief amplitude	30 m SRTM DEM
NDVI	Landsat8 OLI imagery	TWI	30 m SRTM DEM

3. Methodology

In the present work, the influence of different factors on the LSTM model was studied using Landslides_SL. Thereafter, based on the optimal input sequence, SVM, CNN, LSTM and Conv-SE-LSTM models were used to evaluate landslide susceptibility along the Sichuan-Tibet transportation corridor. To analyze the dynamic change in landslide susceptibility on a yearly scale, the susceptibility maps for 2011 and 2016 were generated using the proposed optimal model and the results were evaluated using Landslides_NASA. ArcGIS was the operating software and Python was used for programming. The SVM was implemented using Scikit-learn (https://scikit-learn.org/stable) and CNN, LSTM and Conv-SE-LSTM were implemented in Python under the PaddlePaddle2.0 framework (https://www.paddlepaddle.org.cn). A detailed flowchart is shown in Fig. 4.

3.1. Sub-region division Strategy

The Sichuan-Tibet transportation corridor crosses different types of geological and geomorphic regions with complex geological conditions. In order to evaluate the robustness and generalization of various models, referring to Cui and Zou (2021), the study area was divided into five sub-regions – namely the Minjiang-Dadu River Basin, the Ya-lung River Basin, the Jinsha River Basin, the Salween-Lancang River Basin and the Brahmaputra River Basin (Table 2) – based on the number of water systems, geomorphic units, the disaster mechanism of landslides and the number of landslides in the study area.

The Minjiang-Dadu River Basin lies in the transition zone between the Sichuan Basin and the Qinghai-Tibet Plateau. This region sustains abundant rainfall and possesses various geomorphic features, such as plains, hills, mountains and valleys. The lithology features mainly sandy conglomerate, granite and diorite, located at the intersection of the Xianshuihe, Longmenshan and Anninghe faults, and the exogenic

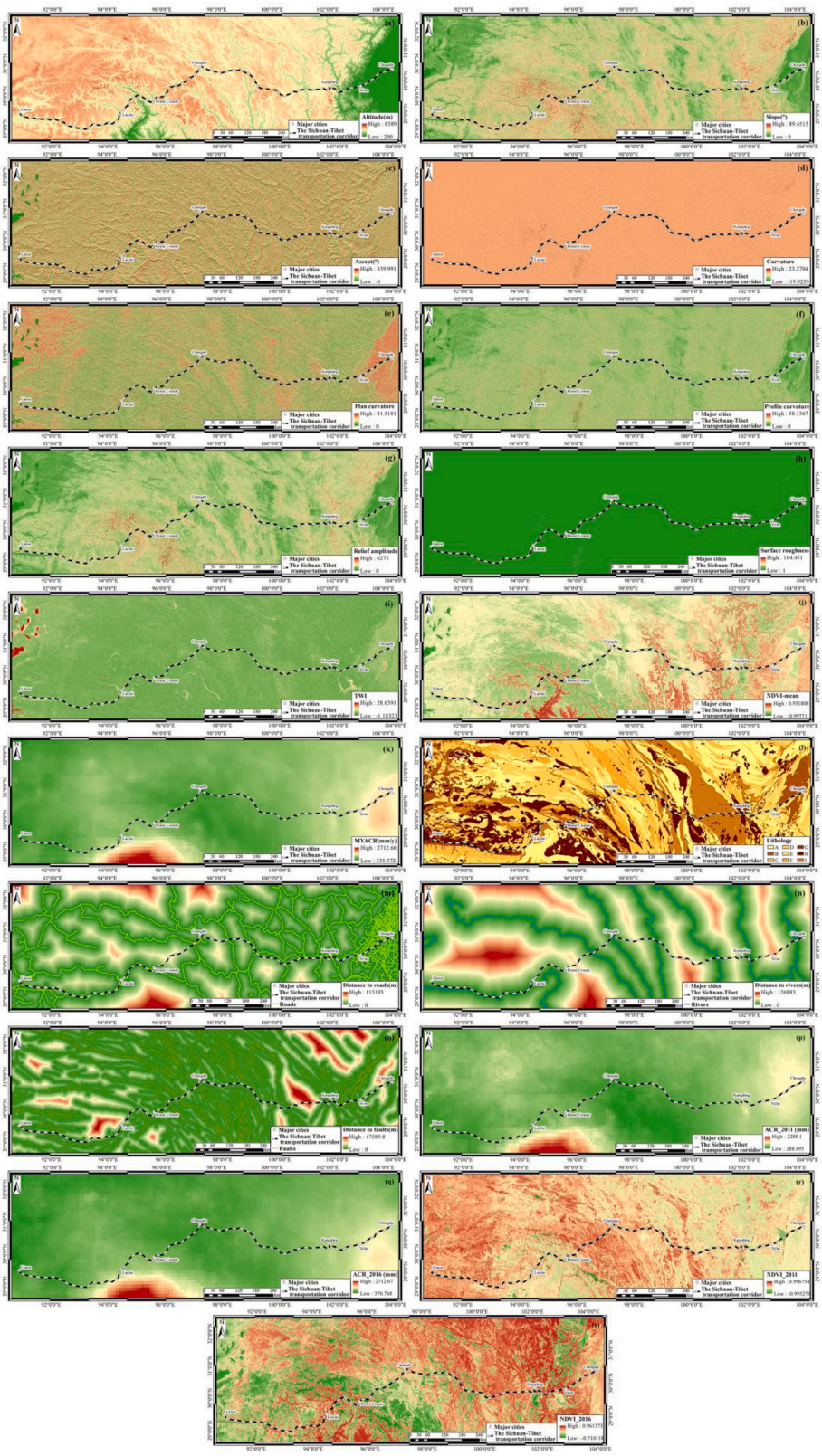

Fig. 2. Landslide conditioning factors along the Sichuan-Tibet transportation corridor: (a) altitude; (b) slope; (c) aspect; (d) curvature; (e) plan curvature; (f) profile curvature; (g) relief amplitude; (h) surface roughness; (i) TWI; (j) NDVI-mean; (k) MYACR; (l) lithology (A-I indicate soft mudstone, mudstone with limestone and gneiss; loose deposits and glacial deposits; soft and hard alternating carbonate and clastic rocks; hard slate and quartz sandstone; hard diabase, olivine and volcanic rocks; soft and hard alternating limestone and marlstone; hard diorite and syenite and basalt; hard granite, andesite and dolomite; soft and hard alternating metamorphic sandstone, marlite and phyllite, respectively); (m) distance to roads; (n) distance to rivers; (o) distance to faults; (p) ACR_2011; (q) ACR_2016; (r) NDVI_2011; and (s) NDVI_2016.

geological process is weak (Cui and Zou, 2021). The Ya-lung River Basin has a relatively open terrain with a lithology of mainly sandy slate and metamorphic rock. This region has been affected by the Xianshuihe fault zone with strong fault activity and weak exogenic geological processes, such as weathering and erosion (Guo et al., 2015). The Jinsha River Basin is dominated by alpine canyon landform, having large ground fluctuations, serious river undercutting erosion and dense landslide distribution. The geological structure is mainly controlled by the Jinsha River fault zone, and the exogenic geological process is strong (Peng et al., 2020). The Salween-Lancang River Basin is located in the Hengduan Mountains and the canyon area in the southeast Tibet. The formation lithology is complex and composed of sandstone and phyllite.

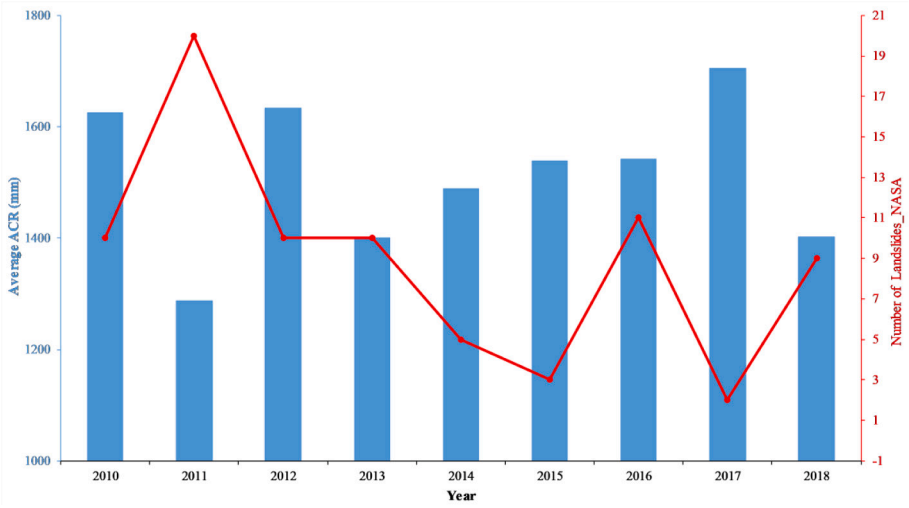

Fig. 3. Average ACR and the number of Landslides_NASA from 2010 to 2018.

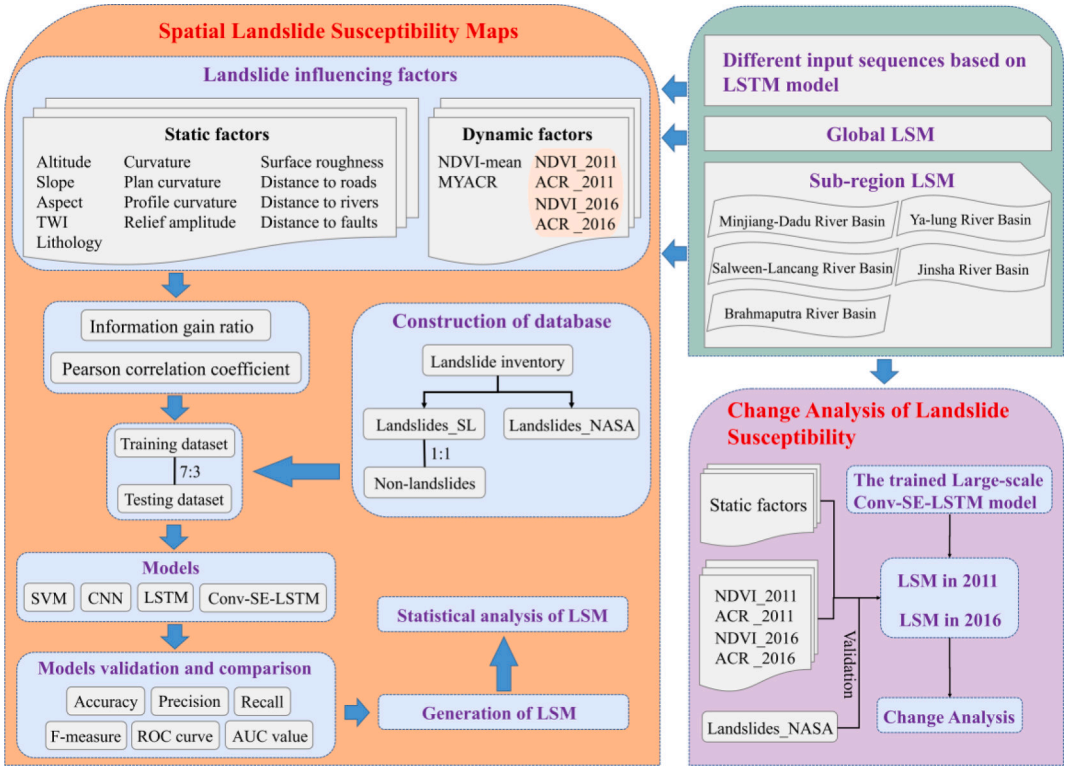

Fig. 4. Flowchart of the present study.

This area is mainly affected by the Lancang River and Salween River fault zones. The faults are active and the exogenic geological process is strong (Cui and Zou, 2021). The Brahmaputra River Basin is dominated by high mountains, deep valleys and river valleys, while the lithology is mainly slate and sandstone. The main fault zone is the Brahmaputra River fault zone with weak fault activity and weak exogenic geological processes (Wu et al., 2020).

3.2. Construction of a spatial database

The construction of the landslide datasets is a vital task in LSM. The occurrence of the landslides depends upon the environmental conditions around the landslides. With reference to the work of Regmi et al., (2013), Wang et al. (2021) and Huang et al. (2022), the 120 m circular buffer zone for the landslide points were constructed, and take the minimum external rectangle of the buffer zone as the sample range. Furthermore, we also created non-landslide datasets using the above-mentioned method. The non-landslide points were randomly selected from a range at least 1 km away from all of the landslide points. In this study, Landslides_SL were used to construct the landslide datasets, and the number of landslides used in each region is shown in Table 3. To improve the accuracy and convergence speed of the model, it is necessary to normalize each conditioning factor layer data to 0 – 1, and the landslide dataset was marked as 1 and the non-landslide dataset as 0.

Notes: ① Global; ② Minjiang-Dadu River Basin; ③ Ya-lung River Basin; ④ Jinsha River Basin; ⑤Salween-Lancang River Basin; and ⑥ Brahmaputra River Basin.

Table 2
Basic information on the sub-regions.

Sub-regions	Main lithology	Climatic conditions	Main fault zone	Exogenic geological process
Minjiang-Dadu River Basin	Sandy conglomerate, granite and diorite	Warm and humid subtropical Pacific southeast monsoon climate, subtropical mountain monsoon climate	Intersection of Xianshuihe, Longmenshan and Anninghe faults, influence of fault activity is slight	Weak
Ya-lung River Basin	Sandy slate and metamorphic rock	Plateau monsoon climate, climate changes with height	Xianshuihe fault zone	Weak
Jinsha River Basin	Granite, syenite and diorite	Plateau monsoon climate, climate changes with height	Jinsha River fault zone	Strong
Salween-Lancang River Basin	Sandstone and phyllite	In dry and hot valley and arid areas, the vertical climate change is obvious	Lancang River and Salween River fault zones	Strong
Brahmaputra River Basin	Slate and sandstone	Combined action of multiple climatic conditions	Brahmaputra River fault zone	Weak

Table 3
Number of landslides in each region.

Zone	Number of landslides	Number of training samples	Number of testing samples
①	1590	1113	477
②	479	335	144
③	154	107	47
④	361	252	109
⑤	323	226	97
⑥	273	191	82

3.3. Evaluation of the conditioning factors

Feature selection is very important for LSM. Redundancy factors will lead to low performance and time-consuming of the model. In this paper, Pearson correlation coefficient (PCC) and Information gain ratio (IGR) were used for feature selection.

If correlation between the landslide conditioning factors is high, it will not only cause data redundancy and reduce the execution efficiency of the model, but will also affect the reliability of the prediction accuracy. The PCC (Chen et al., 2018; Yao et al., 2020) is a statistical parameter which can quantitatively measure the correlation between two variables. When the absolute value of correlation coefficient is greater than or equal to 0.5, there is a strong correlation between the variables, which should be eliminated from the study (Qi et al., 2021; Tien Bui et al., 2016).

To improve the efficiency and accuracy of LSM and reduce the influence of the non-effective factors, the IGR method was used to select the factors that contribute to the occurrence of landslides (Dash and Liu, 1997). The higher the IGR value, the greater the influence of that factor on the occurrence of landslides. If the IGR value is equal to 0, the conditioning factor has no influence on the occurrence of landslides and should be eliminated from the prediction process (Yu et al., 2019).

3.4. Models

3.4.1. SVM

The support vector machine (SVM) is a binary classification model whose purpose is to draw a line to "best" distinguish two types of points on the plane (Awad and Khanna, 2015). The process of the classification of landslides and non-landslides using conditioning factor layers is actually a nonlinear classification process. The SVM introduces a kernel function to map the landslide conditioning factors to higher-dimensional feature spaces. Furthermore, for sample classification, the SVM allows the identification of an optimal hyperplane of the maximum distance between the landslide and non-landslide points from the feature space (Fang et al., 2020; Pradhan, 2013). Xu et al. (2012) discussed the influence of different kernel functions of SVM on LSM. Their results showed that the radial basis kernel function (RBF) used in SVM offered the best prediction performance. Therefore, this paper has chosen RBF as the kernel function with which to construct the SVM model.

The SVM model based on RBF kernel function has two parameters: *gamma* and *C*. The parameter *gamma* defines the influence size of a single training sample and implicitly determines the distribution of the data after mapping to the new feature space. Parameter *C* is the penalty coefficient, which is used to balance the "maximum margin" and the "number of wrong samples". The selection of *gamma* and *C* will have an impact on the performance of the model.

3.4.2. CNN

Convolutional neural networking (CNN) is a deep learning algorithm with the characteristics of local connectivity and shared weights (Sameen et al., 2020; Yang et al., 2021). The structure of a typical CNN comprises an input layer, convolutional layer, pooling layer, fully connected layer and output layer. In a typical convolution operation: first, one or several convolutional layers are used to convolute an image; then, a series of feature maps are down-sampled; finally, these down-sampled feature maps are mapped to the sample labeled space through the fully connected layer. The purpose of the convolution operation is to extract different features from the input layer. The process of down-sampling these feature maps is known as pooling. The most common pooling methods are maximum pooling and average pooling (Fang et al., 2020). Maximum pooling takes the maximum value of the features in a single pooling area, and average pooling takes the average value of the features in a single pooling area. A fully connected layer is used to classify the feature maps and output classification results (Yi et al., 2020).

The CNN model constructed in the study is shown in Fig. 5. The input layer comprised *c* data channels of size $n \times n$. The hidden layer consisted of two convolution layers (*conv1* and *conv2*) and two maximum pooling layers (*pool1* and *pool2*). The number of convolution kernels in *conv1* and *conv2* were 64 and 132, respectively. Furthermore, the sizes of the convolution kernel and the pooling layer were 3×3 and 2×2, respectively. Also, a 0 element was used to fill in the convolution to ensure that the feature space retained its size after convolution. A *dropout* layer was added after each pooling layer to prevent over-fitting and achieve a regularisation effect to a certain extent. *fc* is the full connection layer. The final output layer output two neurons through the *softmax* activation functions, 0 and 1, where 0 represents non-landslide and 1 represents landslide.

3.4.3. LSTM

A long short-term memory network (LSTM) is a special structure of recurrent neural networking (RNN) used to solve the problem of long-term dependence information. LSTM was first proposed by Hochreiter and Schmidhuber, (1997), and then improved by Graves, (2012). LSTM

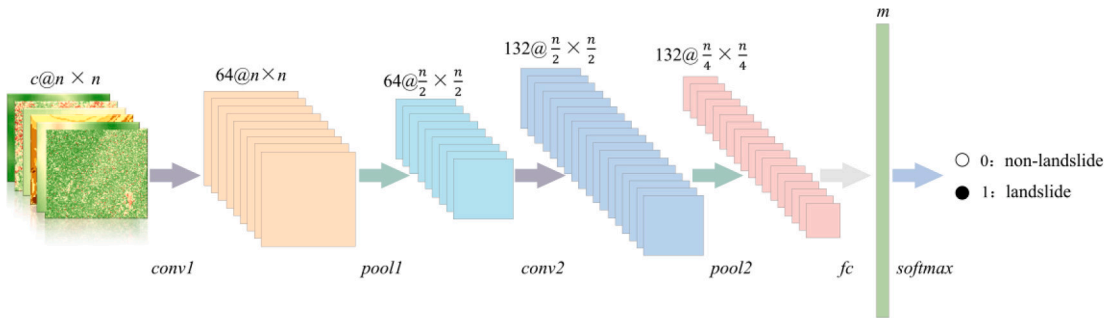

Fig. 5. CNN model structure.

takes the output of the previous layer as the input of the next layer (Mutlu et al., 2019). Therefore, it uses the previous historical information and the adjacent historical information for model training, and shows good performance in dealing with sequence problems. Different factor input sequences will affect the performance of the LSTM model. The impact of different sequence inputs on the LSTM model is discussed in Section 4.2, and the optimal input sequence suitable for LSM is given. Each LSTM cell has four layers, namely-three sigmoid layers and a *tanh* layer. The transfer of information is controlled by three gates (Shi et al., 2015): ① the forget gate: this contains a sigmoid layer, which is used to determine how much information is forgotten with respect to the input (x_t) at time t and hidden output (h_{t-1}) at the previous time; ② the input gate: this contains a sigmoid layer and a *tanh* layer and is used to control how much information of candidate internal states (C_{t-1}) is reserved according to the input (x_t) at time t and hidden output (h_{t-1}) at the previous time; and ③ the output gate: this contains a sigmoid layer,

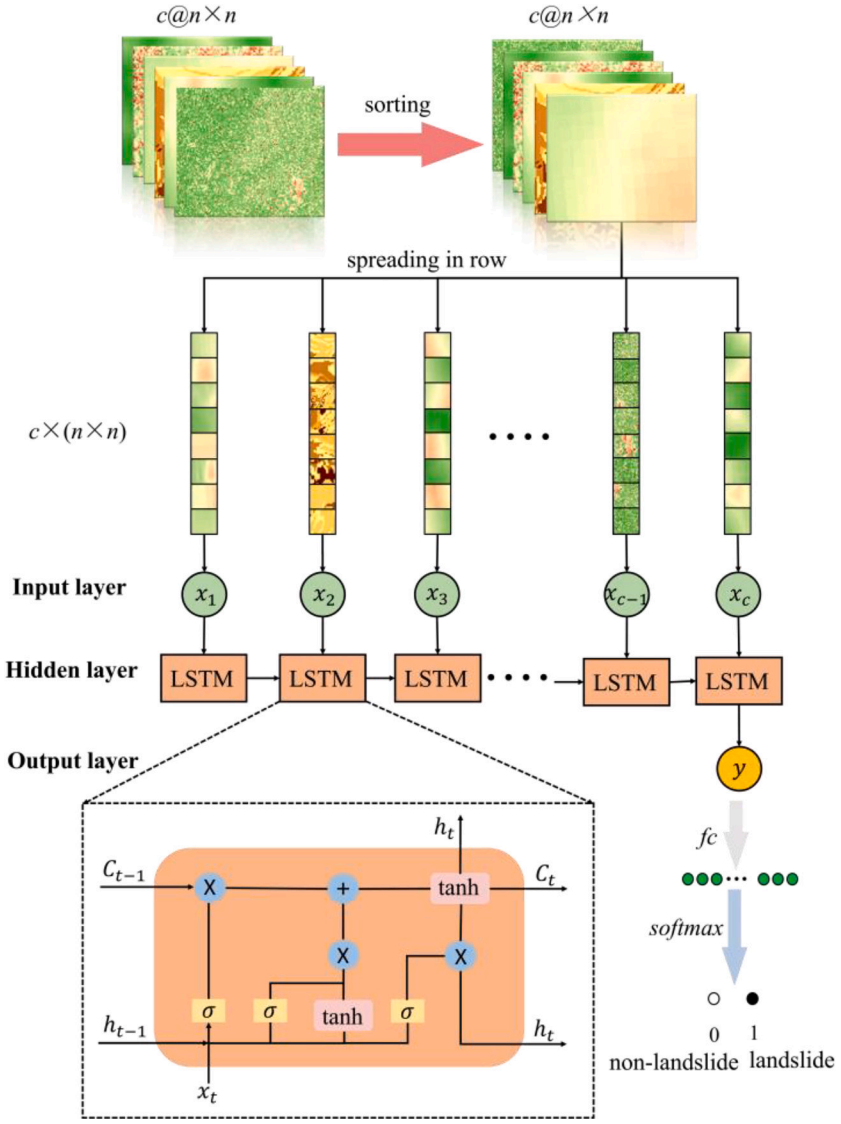

Fig. 6. LSTM model structure.

which is used to determine the output value of the hidden output (h_t) and the candidate internal state (C_t) at time t.

The LSTM structure is shown in Fig. 6. First, c data channels of size $n \times n$ were sorted into a certain sequence. Each factor layer is thus a two-dimensional matrix with size $c \times (n \times n)$. Each column represents a different factor layer data. Each row represents a level of factor layer data. The top factors in the sequence were introduced first to the model, whereas the bottom factors in the sequence were input last. The final output layer output two neurons through *softmax* activation functions, 0 and 1, where 0 is non-landslide and 1 is landslide.

3.4.4. Proposed Conv-SE-LSTM

The proposed Convolutional-Squeeze and Excitation-long short term memory network (Conv-SE-LSTM) model consists of convolution module, SE attention module and LSTM module. Firstly, the model extracts useful deep features from multi-channel factor images through convolution module. Then, the SE attention module adaptively obtains the importance of each extracted feature channel. The features with different weights are input into the LSTM module with an optimal sequence. Finally, the probability of landslide in evaluation unit could be obtained by classification layer.

The SE attention module starts with a squeeze operation. Global average pooling was used to compress each two-dimensional feature channel into a real number in the spatial dimension. The output dimension is consistent with the input feature channel number. In the exception operation, two fully connected layers were used to adaptively generate weights for each feature channel. Next, the obtained weights were weighted to the previous features through scale operation to recalibrate the original features in the channel dimension. It is noteworthy that the higher the correlation between the channel and key information, the greater the weight becomes. The learned weight was then assigned to the original feature graph to enhance those features useful to the current task and suppress those features that were less useful (Hou et al., 2021; Hu et al., 2020).

The proposed Conv-SE-LSTM model can solve the problem of long-term dependence so that most of the critical information about the occurrence of a landslide is retained and transferred to the next hidden state to assist in judgment. At the same time, it also can adaptively obtain the importance of each feature channel through learning, emphasize effective information, suppress invalid information, and improve network performance.

The Conv-SE-LSTM model framework is shown in Fig. 7. First, c factor layers of size $n \times n$ were sorted into a certain sequence. Then, a group convolution with three convolution kernels was used for each factor layer. The size of the convolution kernel was 3×3 and the step size was 2 so that three $(floor(\frac{n}{2}) + 1) \times (floor(\frac{n}{2}) + 1)$ feature maps could be obtained. The feature maps were then stacked into the characteristic graph of size $(3 \times c) \times (floor(\frac{n}{2}) + 1) \times (floor(\frac{n}{2}) + 1)$, which became $(3 \times c) \times 1 \times 1$ after squeeze. The exception operation was used to adaptively calculate the weight, whereas the scale operation was conducted to weight the obtained weight to the previous features and further obtain a $(3 \times c) \times (floor(\frac{n}{2}) + 1) \times (floor(\frac{n}{2}) + 1)$ size weighted characteristic graph. The c channels were reshaped to one dimensional vectors of size $3 \times (floor(\frac{n}{2}) + 1) \times (floor(\frac{n}{2}) + 1)$. They were stacked into a matrix of size $c \times (3 \times (floor(\frac{n}{2}) + 1) \times (floor(\frac{n}{2}) + 1))$ images in a certain sequence. These matrices were input into the LSTM network model line by line. The final output layer output two neurons through *softmax* activation function, 0 and 1, where 0 is non-landslide and 1 is landslide.

3.5. Model evaluation and Comparison

Accuracy, precision, recall, F-measure, receiver operating characteristic (ROC) and area under curve (AUC) were used to evaluate the prediction ability of the model. LSM is equivalent to a two-classification problem, where the output results are only landslide and non-landslide.

Table 4
The confusion matrix.

Classification	Predicted results	Actual results
True positive (TP)	landslide	landslide
False positive (FP)	landslide	non-landslide
True negative (TN)	non-landslide	non-landslide
False negative (FN)	non-landslide	landslide

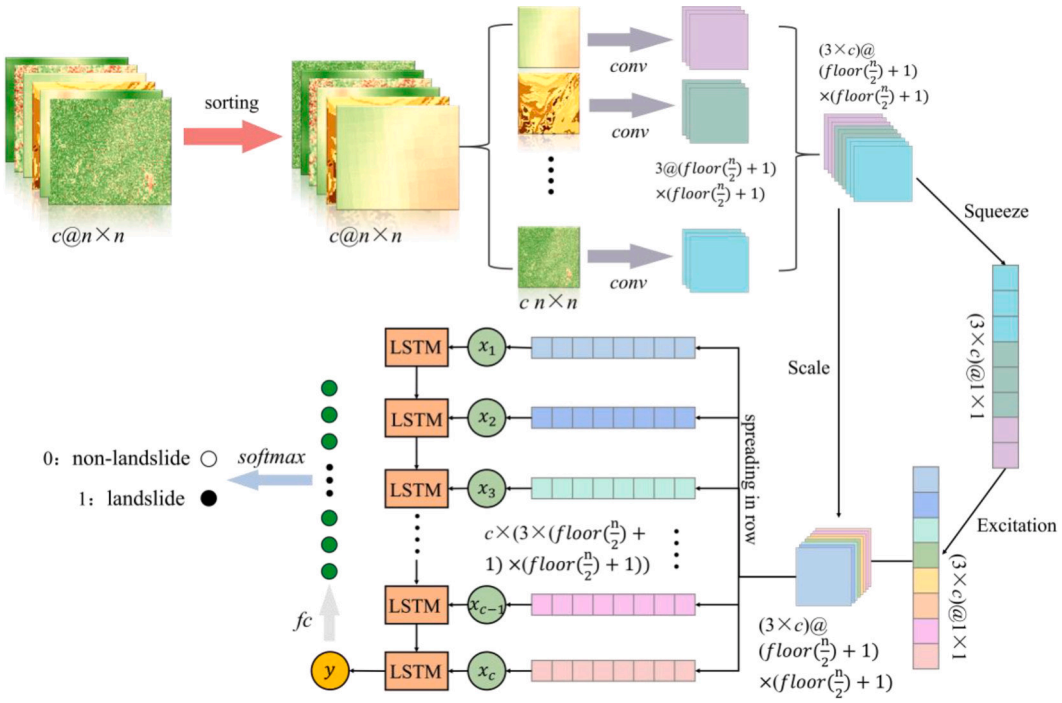

Fig. 7. Conv-SE-LSTM model structure.

Table 4 shows the confusion matrix was constructed according to different combinations of real value and predicted value. If both the actual and predicted results are landslide, it is a true positive (TP); if both the actual and predicted results are non-landslide, it is a true negative (TN); if the predicted result is non-landslide but the actual result is landslide, it is a false negative (FN); and if the predicted result is landslide but the actual result is non-landslide, it is a false positive (FP).

Accuracy (Acc), precision, recall, *F*-measure (Fang et al., 2020; Ji et al., 2020) are calculated as follows:

$$Acc = \frac{TN + TP}{TN + TP + FP + FN} \tag{1}$$

$$Precision = \frac{TP}{TP + FP} \tag{2}$$

$$Recall = \frac{TP}{TP + FN} \tag{3}$$

$$F - \text{measure} = \frac{2 \times P \times R}{P + R} = \frac{2 \times TP}{2 \times TP + FP + FN} \tag{4}$$

ROC curve and AUC have been widely used in the performance evaluation of landslide susceptibility models (Al-Najjar and Pradhan, 2021; Dao et al., 2020; Rabby et al., 2020). In the ROC curve (Hanley and McNeil, 1982), the false positive rate (FPR) is the *x*-axis, and the

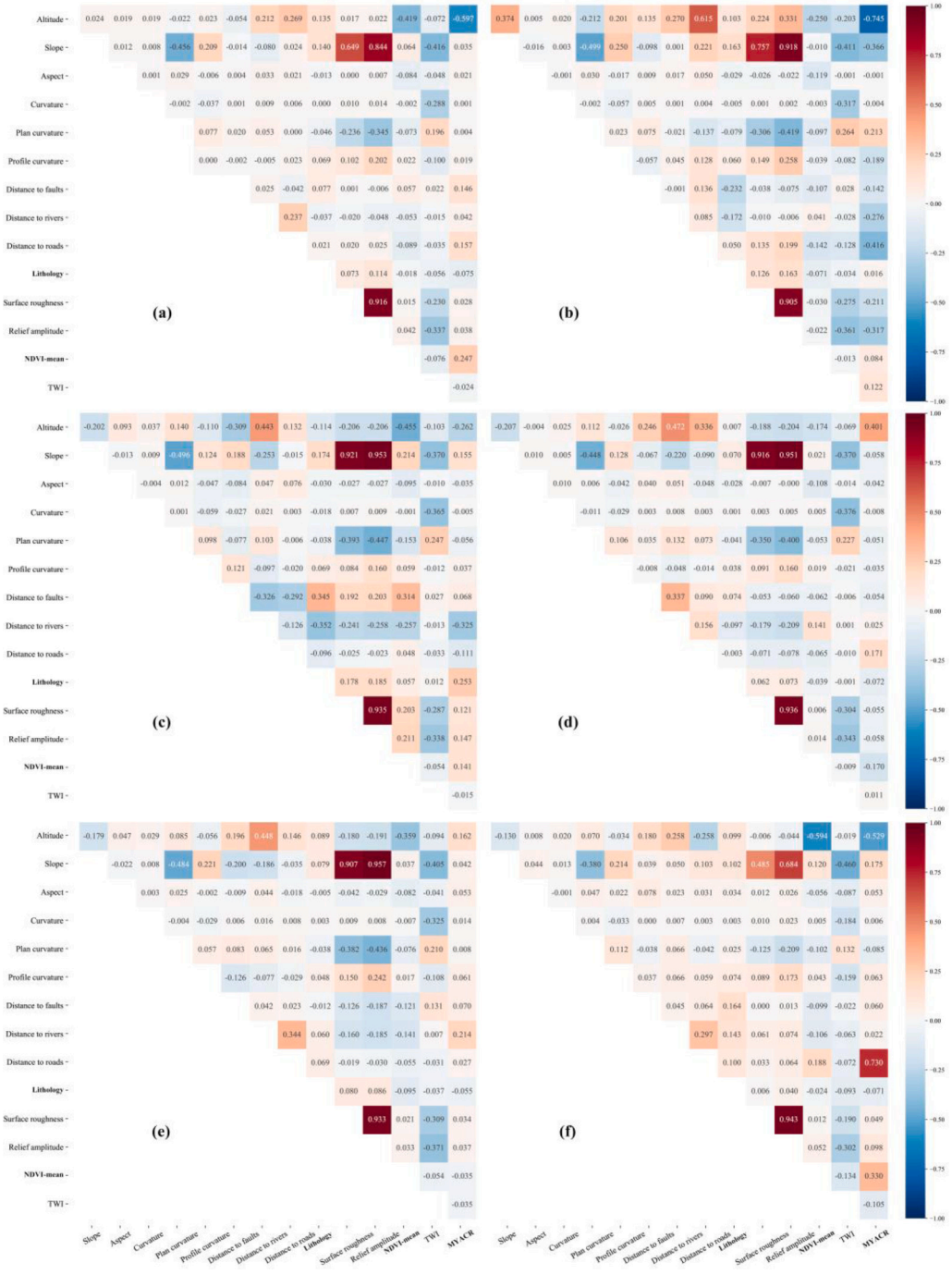

Fig. 8. Pearson correlation coefficient matrixes: (a) Global; (b) Minjiang-Dadu River Basin; (c) Ya-lung River Basin; (d) Jinsha River Basin; (e) Salween-Lancang River Basin; and (f) Brahmaputra River Basin.

true positive rate (TPR) is the *y*-axis. At the same time, the area under ROC (AUC) was used to quantitatively evaluate the prediction accuracy of the methods. The AUC value range is [0,1]. The larger the AUC value, the higher the accuracy of the model classification and the better the accuracy.

$$\mathrm{FPR} = \frac{FP}{FP + TN} \tag{5}$$

$$TPR = \frac{TP}{FN + TP} \tag{6}$$

4. Results

The landslide susceptibility mapping of the areas along the Sichuan-Tibet transportation corridor was carried out from the perspectives of global and sub-regions to verify the performance of our proposed Conv-SE-LSTM model. The steps applied to verify the performance involved: (1) selecting landslide conditioning factors to improve the performance of the model; (2) fully mining the optimal factor input sequence for LSTM model; (3) spatial analysis of LSM; and (4) calculating ACC, precision, recall, F–measure, AUC value and ROC curve to evaluate the performance of the model. Finally, LSM with dynamic factor changes under the optimal model was achieved.

4.1. Selection of landslide conditioning factors

The calculation results of PCC and IGR values of landslide conditioning factors along the Sichuan-Tibet transportation corridor are shown in Figs. 8 and 9, respectively. Fig. 8(a) shows the correlation between altitude and MYACR is slightly higher than 0.5. This is because most areas along the Sichuan-Tibet transportation corridor are mountainous areas. The rainfall increases with the increase of altitude from the foot of the mountain. After reaching a certain height, the rainfall decreases with the increase of altitude. At the same time, the correlation coefficient between slope and surface roughness is much higher than 0.5, because the greater the slope, the more severe the soil erosion. And the more complex the surface morphology, the greater roughness and relief amplitude of the surface. Fig. 9 dark green line shows the IGR calculation results in the global research of the Sichuan-Tibet transportation corridor. It can be seen that the IGR value of the MYACR is higher than the altitude, and the IGR value of the slope is higher than the relief amplitude and surface roughness. Therefore, the three conditioning factors of altitude, relief amplitude and surface roughness were removed according to the principle of higher correlation and less importance between factors and the remaining 12 were applied to the global research of the Sichuan-Tibet transportation corridor. Similarly, in the case of the Minjiang-Dadu River Basin, altitude, relief amplitude and surface roughness were removed, and the remaining 12 factors were used for the study. For the Ya-lung River Basin, Jinsha River Basin and Salween-Lancang River Basin, relief amplitude and surface roughness were removed, and the remaining 13 factors were utilized. Finally, in the case of the Brahmaputra River Basin, altitude, distance to roads and relief amplitude were not considered and the remaining 12 factors were used.

A comprehensive analysis of the calculation results revealed that, for all the zones, the correlation coefficients between relief amplitude and surface roughness, relief amplitude and slope were very high. The IGR of MYACR was the largest value in all regions in the study area and was significantly higher than all other factors. By contrast, the IGR values of relief amplitude and curvature were lower than the other factors, indicating that these two factors have little impact on the occurrence of landslides. The factors removed for different sub-regions were different, and the contribution values of each factor to the occurrence of landslides in different sub-regions were also different. This showed that the sub-regions were different to each other and demonstrated a necessity for zone mapping.

4.2. Comparisons of different factor input sequences based on LSTM model under global evaluation

The LSTM model can fully mine the sequence information between the factors, with the most critical information contributing to landslides occurrence being retained and passing to the next hidden state. Wang et al. (2020) proposed a sequential data representation method of landslide conditioning factors in which the factors are sorted in descending order of importance, calculated by the information gain ratio method. However, they did not compare the performance of this input sequence with other input sequences. The present paper discusses the effects of three different sequence representations on the performance of the LSTM model. The three sequence representations are: ① sorted in descending order of importance calculated by the information gain ratio method; ② sorted in increasing order of importance calculated by the information gain ratio method; and ③ sorted in random order based on topography, geology, rainfall and human activity.

According to the IGR results calculated in Section 4.1, the above three sequence inputs are shown in Table 5. Three different sequences were input into the LSTM model and tuned to obtain optimal results. Table 5 shows the optimal AUC results of the three different sequence representations. The results showed that the AUC value of the first input factor sequence was the highest, indicating that the input factor

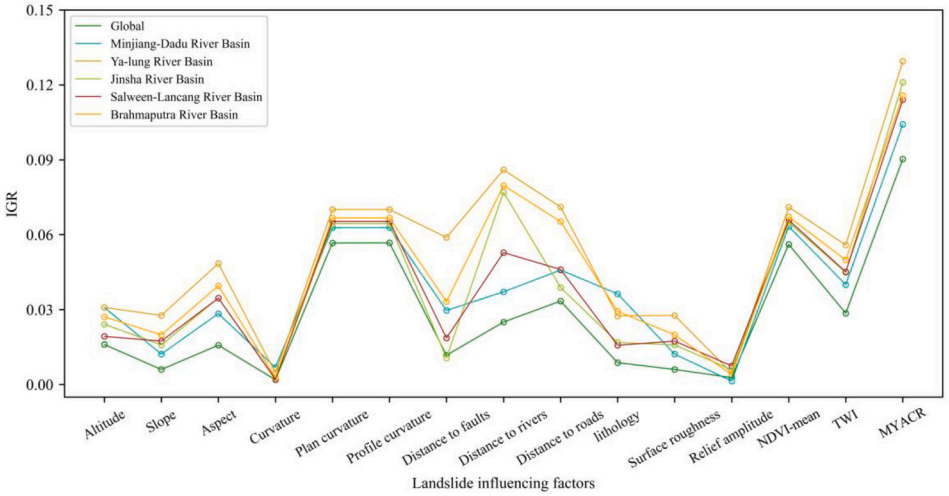

Fig. 9. Information gain ratio results.

Table 5
Sequential data representation results based on three methods.

Method	Input sequential data	AUC
①	Rainfall, profile curvature, plan curvature, NDVI, TWI, distance to rivers, distance to faults, aspect, distance to roads, lithology, slope, curvature	0.8484
②	Curvature, slope, lithology, distance to roads, aspect, distance to faults, distance to rivers, TWI, NDVI, plan curvature, profile curvature, rainfall	0.8399
③	Slope, aspect, curvature, profile curvature, plan curvature, TWI, lithology, distance to faults, rainfall, distance to rivers, distance to roads, NDVI	0.8448

sequence is more suitable for the LSTM model and can improve the performance of the model. The first input factor was followed sequentially by the third and then the second input factors. The optimal sequence data input first introduces the relatively important factors into the LSTM structure and is retained, and then passes them to the next hidden state to continue to affect the judgment of the model. The least important factors are finally introduced into the model, so as to obtain more accurate LSM results.

4.3. Generation of landslide susceptibility maps

In this subsection, the four methods introduced in Section 3.4 are used for landslide susceptibility analysis. All the model parameters are optimized by trial-and-error method, the selected groups of parameters are trained and the optimal result is selected. For CNN, LSTM and Conv-SE-LSTM, the middle layer activation function uses '*ReLU*'. '*ReLU*' activation function is one of the most commonly used and effective activation functions. It has two main advantages: (1) it overcomes the problem of gradient disappearance, (2) compared with other activation functions, it is more effective for training prediction methods (Wang et al., 2021; Wang et al., 2019). The optimizer uses '*Adam*', the input layer c is the number of conditioning factors selected, $n = 8$. The parameter settings of the different models are shown in Table 6.

The trained model was used to predict the evaluation units, and a susceptibility index for each evaluation unit was obtained to produce the LSM. The susceptibility indexes predicted by SVM, CNN, LSTM and Conv-SE-LSTM were all between 0 and 1. The larger the susceptibility index, the more likely the landslide is to occur in the area; otherwise, a landslide is less likely to occur.

4.3.1. Global landslide susceptibility mapping

The generated susceptibility map was reclassified using the natural break method into five grades: very low, low, moderate, high and very high. Fig. 10 shows the landslide susceptibility maps along the Sichuan-Tibet transportation corridor obtained by SVM, CNN, LSTM and Conv-SE-LSTM.

The landslide frequency ratio (Yu et al., 2019) is the ratio between the number of landslide points falling into a certain susceptibility grade in a certain area and the proportion of the grade area within the total area, and can be used to measure the accuracy of LSM. The landslide frequency ratio was calculated for each class of the susceptibility map, as shown in Fig. 11.

Fig. 10 shows that the very high susceptibility areas along the Sichuan-Tibet transportation corridor are mainly concentrated on both sides of the Ya-lung River, the Jinsha River, the Lancang River, the Salween River and the Brahmaputra River, and on both sides of the roads near Chengdu. It can be seen that the total of high and very high susceptibility areas predicted by the SVM model exceeded that predicted by the other models. The prediction results of CNN, LSTM and Conv-SE-LSTM models were very similar. In excess of half of the study area was marked as very low and low susceptibility areas, and most of the landslides were located in high and very high susceptibility areas. Few landslides were located in very low susceptibility areas, which is in line with the actual situation.

Table 6
Model parameter settings along the Sichuan-Tibet transportation corridor.

Zone	Models	Parameter settings		
①	SVM	Kernel Function: RBF	C: 1	gamma: 0.005
	CNN	dropout-1: 0.5 Epoch: 769 Learn rate: 0.0001	dropout-2: 0.5 Batch size: 64	m: 350 Buffer size: 650
	LSTM	Epoch: 492 Learn rate: 0.0001	Batch size: 32 m: 200	Buffer size: 650
	Conv-SE-LSTM	Epoch: 1499 Learn rate: 0.0001	Batch size: 64 m: 200	Buffer size: 500
②	SVM	Kernel Function: RBF	C: 5	gamma: 0.005
	CNN	dropout-1: 0.5 Epoch: 471 Learn rate: 0.0001	dropout-2: 0.5 Batch size: 32	m: 350 Buffer size: 1000
	LSTM	Epoch: 633 Learn rate: 0.0001	Batch size: 64 m: 200	Buffer size: 800
	Conv-SE-LSTM	Epoch: 1041 Learn rate: 0.0001	Batch size: 32 m: 200	Buffer size: 500
③	SVM	Kernel Function: RBF	C: 1	gamma: 0.01
	CNN	dropout-1: 0.5 Epoch: 967 Learn rate: 0.0001	dropout-2: 0.5 Batch size: 64	m: 350 Buffer size: 800
	LSTM	Epoch: 582 Learn rate: 0.0001	Batch size: 32 m: 200	Buffer size: 500
	Conv-SE-LSTM	Epoch: 1998 Learn rate: 0.0001	Batch size: 64 m: 200	Buffer size: 750
④	SVM	Kernel Function: RBF	C: 0.5	gamma: 0.02
	CNN	dropout-1: 0.5 Epoch: 368 Learn rate: 0.0001	dropout-2: 0.5 Batch size:32	m: 350 Buffer size: 500
	LSTM	Epoch: 494 Learn rate: 0.0001	Batch size: 32 m: 200	Buffer size: 1000
	Conv-SE-LSTM	Epoch: 979 Learn rate: 0.0001	Batch size: 32 m: 200	Buffer size: 900
⑤	SVM	Kernel Function: RBF	C:2	gamma: 0.005
	CNN	dropout-1: 0.5 Epoch: 1199 Learn rate: 0.0001	dropout-2: 0.5 Batch size: 64	m: 350 Buffer size: 1000
	LSTM	Epoch: 893 Learn rate: 0.0001	Batch size:64 m: 200	Buffer size: 700
	Conv-SE-LSTM	Epoch: 1985 Learn rate: 0.0001	Batch size: 64 m: 200	Buffer size: 700
⑥	SVM	Kernel Function: RBF	C: 1	gamma: 0.001
	CNN	dropout-1: 0.5 Epoch: 352 Learn rate: 0.0001	dropout-2: 0.5 Batch size: 64	m: 350 Buffer size: 800
	LSTM	Epoch: 726 Learn rate: 0.0001	Batch size: 64 m: 200	Buffer size: 700
	Conv-SE-LSTM	Epoch:524 Learn rate: 0.0001	Batch size: 64 m: 200	Buffer size: 750

Notes: ① Global; ② Minjiang-Dadu River Basin; ③ Ya-lung River Basin; ④ Jinsha River Basin; ⑤ Salween-Lancang River Basin; and ⑥ Brahmaputra River Basin.

Fig. 11 shows that, with increased landslide susceptibility grade, the landslide frequency ratio also increases, and the frequency ratio in very high susceptibility areas is much higher than that in very low susceptibility areas. At the same time, the difference in frequency ratio between different classes of the susceptibility map predicted by the Conv-SE-LSTM was the largest, followed by the LSTM model, while the difference predicted by the SVM was the smallest. This shows that the

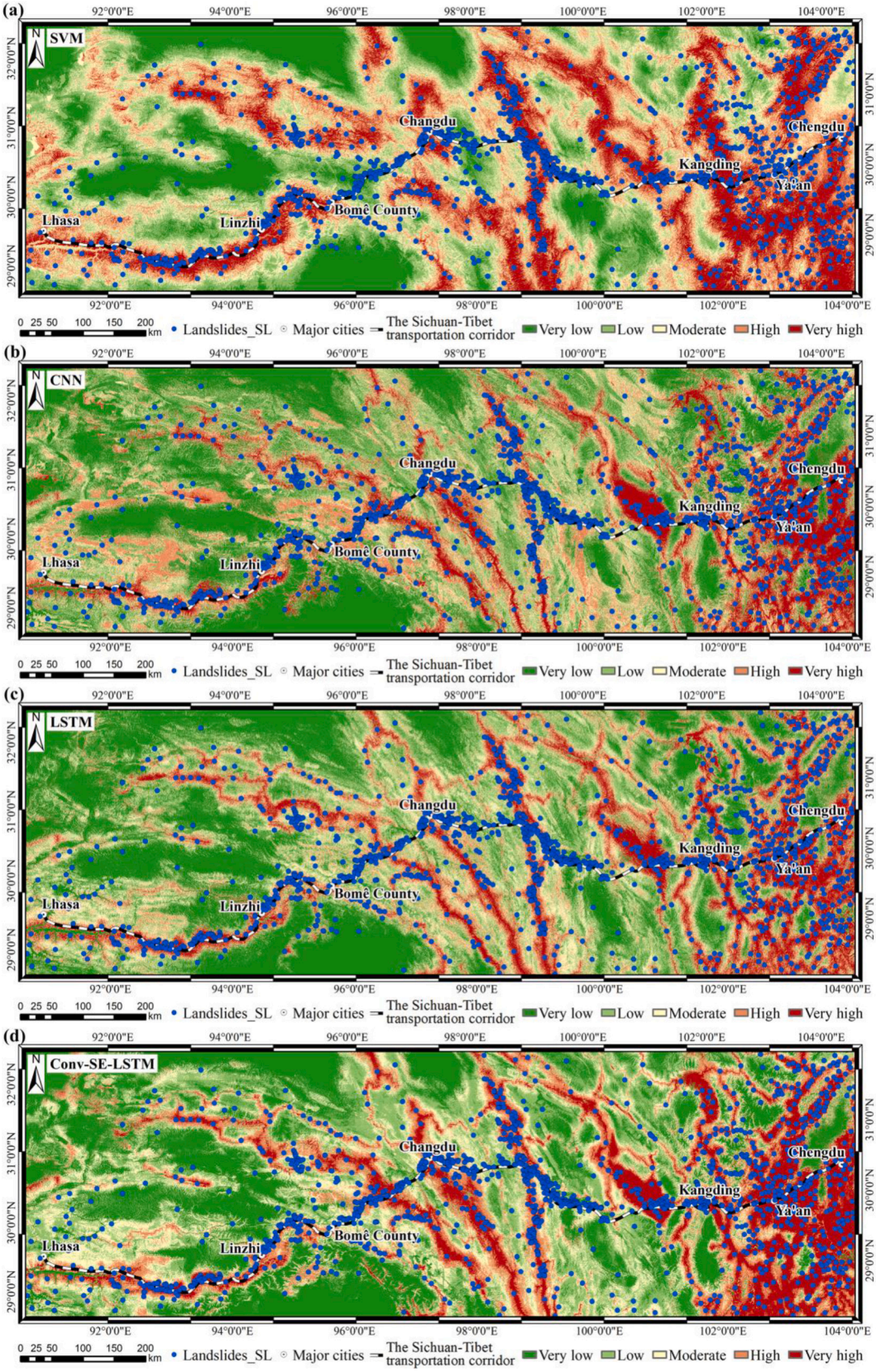

Fig. 10. Landslide susceptibility maps obtained from four models along the Sichuan-Tibet transportation corridor: (a) SVM; (b) CNN; (c) LSTM; and (d) Conv-SE-LSTM.

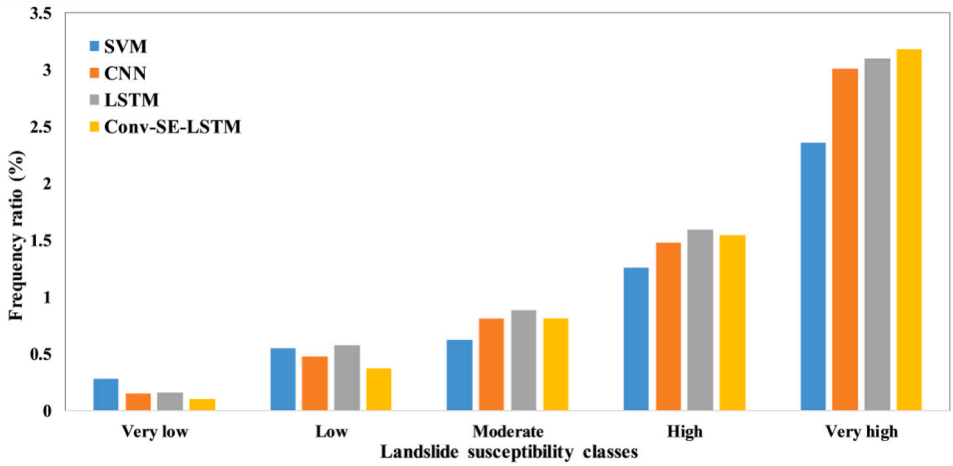

Fig. 11. Landslide frequency ratio of each susceptibility class obtained from four models along the Sichuan-Tibet transportation corridor.

predicted results of the Conv-SE-LSTM model have greater discrimination. In other words, the proposed model offers enhanced prediction.

4.3.2. *Sub-region landslide susceptibility mapping*

The 20 trained sub-regional models were used to predict the corresponding sub-regions. Using the natural break method, the LSM was divided into five grades, namely very low, low, moderate, high and very high (Fig. 12). It can be seen that most of the landslide points are located in high and very high susceptibility areas, and the prediction results of different models in the same sub-region are similar. Compared with the global predicted results, the distribution of very high susceptibility areas is roughly the same. With the exception of the Brahmaputra River Basin, the prediction results for the zones show good continuity. At the same time, the proportion of low and very low susceptibility areas obtained by way of zoning increase significantly, and the distribution of high susceptibility areas becomes more concentrated. In the upper reaches of the Salween River, the susceptibility index of zoning prediction is lower than that of the global prediction. In the Brahmaputra River Basin, there are few sample points and a large zoning area; therefore, the high and medium susceptibility areas predicted by zoning increase significantly, and continuity at the junction with the Salween-Lancang River Basin is poor.

To make the results comparable, the sub-region prediction results and the corresponding global prediction results were divided into five grades in accordance with the equidistant classification method, and the landslide frequency ratio in the five grades was counted (see Fig. 13). It is observed that in the Minjiang-Dadu River Basin and the Jinsha River Basin, the landslide frequency ratio from each model for each sub-region is largely identical. In the case of the Ya-lung River Basin, with the exception of SVM, the landslide frequency ratio from the models for each sub-region is largely identical. For the Salween-Lancang and Brahmaputra River Basins, the landslide frequency ratios from each model for each sub-region are quite different. However, in each basin, the landslide frequency ratio positively correlates with the landslide susceptibility grade. The higher the susceptibility grade, the greater the landslide frequency ratio. This indicates that the zoning prediction results have certain reliability.

4.4. *Validation and comparisons of models*

In Table 7, ① lists the ACC, precision, recall, F-measure values and AUC values of the SVM, CNN, LSTM and Conv-SE-LSTM models along the Sichuan-Tibet transportation corridor. Fig. 14(a) plots the ROC curves using the testing dataset. Conv-SE-LSTM has the highest ACC value (0.8040) and F-measure value (0.8025). This is followed by LSTM, CNN and SVM. SVM has the lowest ACC and F-measure values. Also, Conv–SE-LSTM displays a higher AUC value than the other three models, indicating that Conv-SE-LSTM offers the best predictive performance. The AUC of the Conv–SE–LSTM model is approximately 3 %, 4 % and 8 % higher than that of the CNN model, LSTM model and SVM model, respectively. The SVM model displays the most inferior predictive performance.

In order to make the results comparable, the trained global model and sub-region models were used to predict the testing datasets for each sub-region, and the ACC, precision, recall, F-measure and AUC values were calculated, as shown in Table 7. The ROC curve is shown in Fig. 14. It can be seen that, for each sub-region, the AUC value of the optimal model was higher than 80 %, indicating that the final prediction result of the model is highly reliable.

For the Minjiang-Dadu River Basin, the Jinsha River Basin and the Salween-Lancang River Basin, the AUC value of the proposed Conv-SE-LSTM model was slightly higher than that of the other three models. For the Ya-lung River Basin and the Brahmaputra River Basin, the AUC value of the CNN model was slightly higher than that of the other three models. However, the difference in the AUC values between the CNN and Conv–SE–LSTM models was only around 1 %, implying no significant difference between the model performance. For the SVM model, the sub-region prediction results were slightly better than the global prediction results. Conversely, the global prediction results of other models were slightly better than the sub-region prediction results.

4.5. *LSM under different dynamic factors*

The trained global Conv-SE-LSTM model was used to generate landslide susceptibility maps for 2011 and 2016 in the study area. Fig. 15 shows these maps and the locations of landslide points in the corresponding years. It can be seen that the susceptibility map for different years also changes with changes in rainfall and NDVI; the susceptibility index of most regions shows no significant change, and the regions with large changes are mainly concentrated in the Salween River Basin and the Chengdu-Kangding section. In the natural break method, a susceptibility index greater than 0.555 in 2011 was considered to depict high and very high susceptible areas, and in 2016 a susceptibility index greater than 0.543 was considered to depict high and very high susceptible areas. Such predictions are considered to be correct, and monitoring should be strengthened. Fig. 16 shows the susceptibility index corresponding to landslide points in 2011 and 2016. It can be seen that 19 of the 20 landslides in 2011 and 11 of the 12 landslides in 2016 were predicted accurately, with approximately 93.33 % accuracy. These results show that the method proposed in this paper, which uses the deep learning model to generate a susceptibility map for different ACR and NDVI values, has certain reliability.

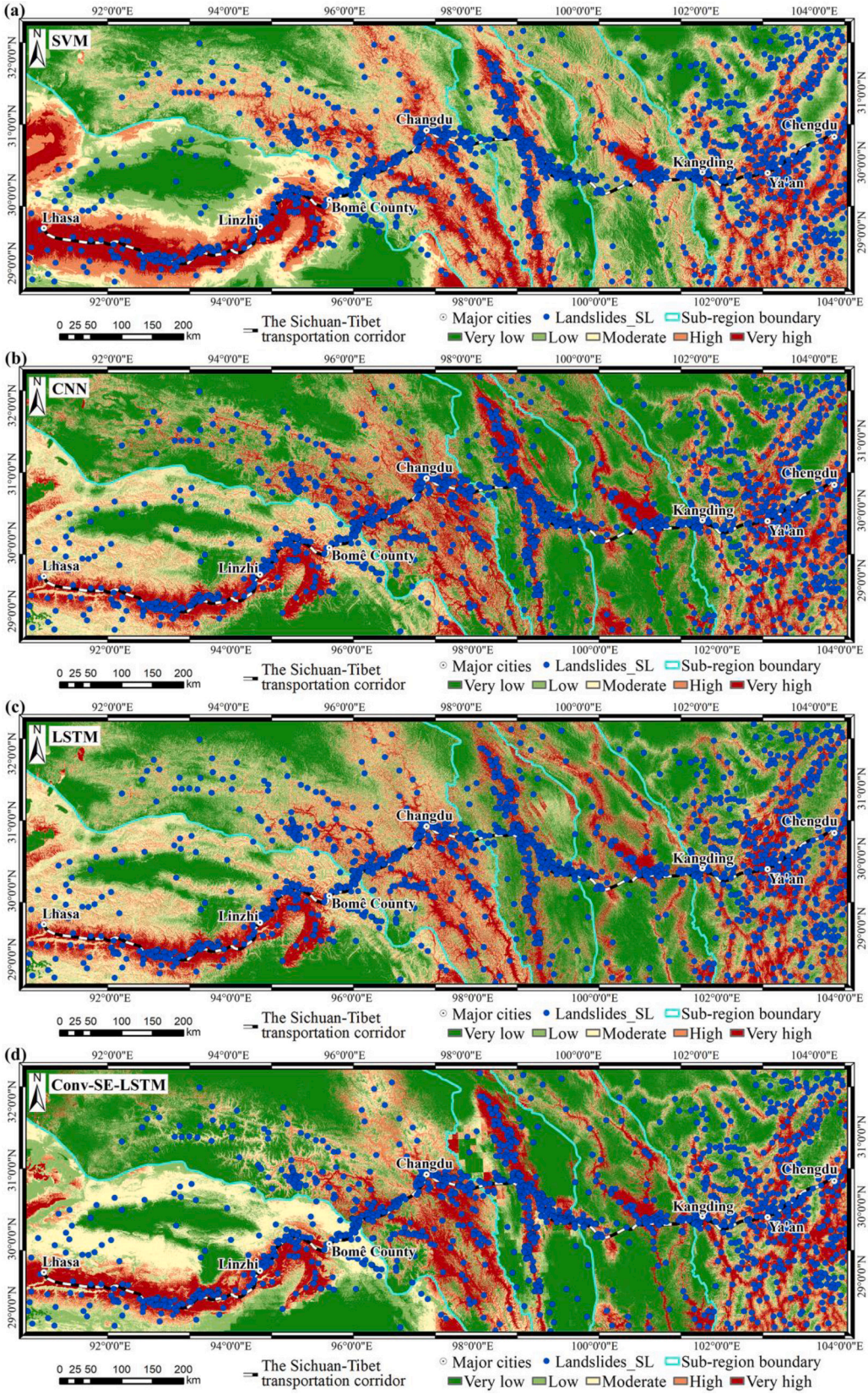

Fig. 12. Landslide susceptibility maps in sub-regions obtained from four models along the Sichuan-Tibet transportation corridor: (a) SVM; (b) CNN; (c) LSTM; and (d) Conv-SE-LSTM.

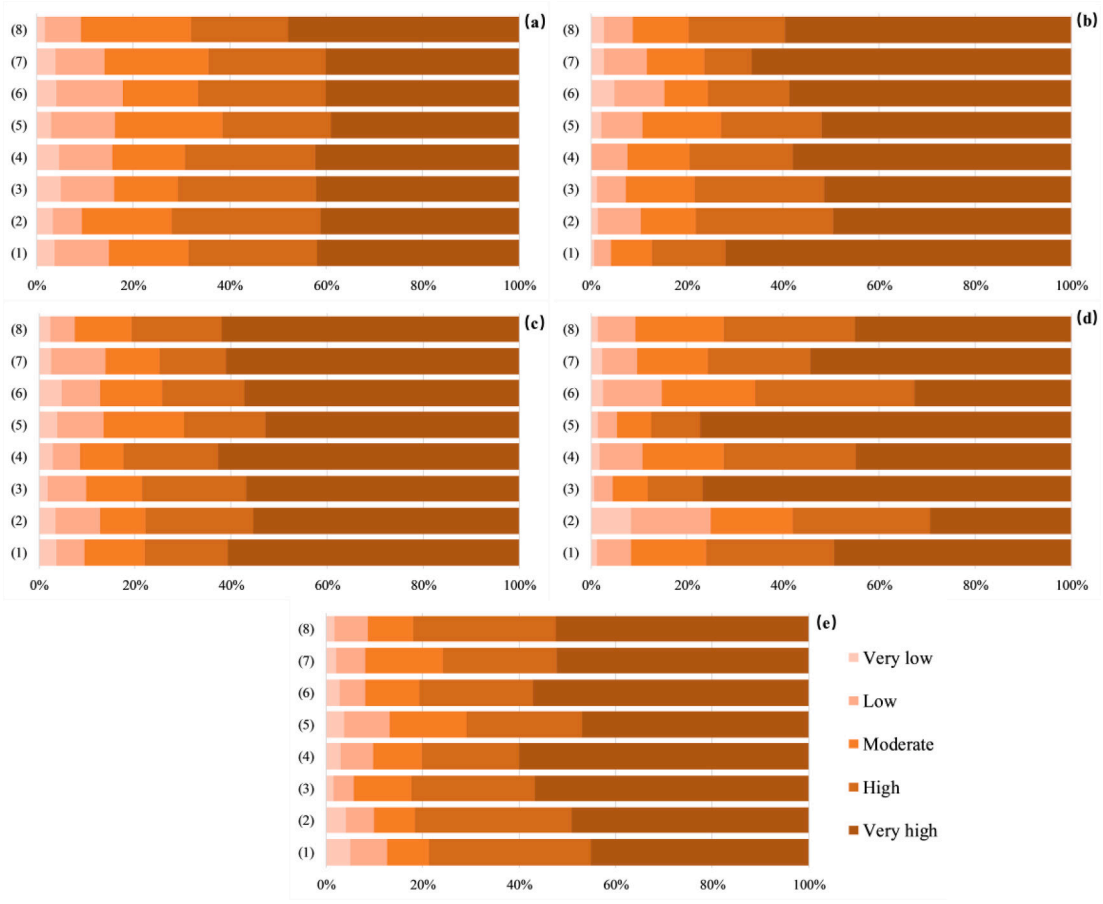

Fig. 13. Statistical results of the proportion of landslides in each susceptibility classification: (a) Minjiang-Dadu River Basin; (b) Ya-lung River Basin; (c) Jinsha River Basin; (d) Salween-Lancang River Basin; and (e) Brahmaputra River Basin. Notes: (1) SVM-sub-regions; (2) SVM-global; (3) CNN-sub-regions; (4) CNN-global; (5) LSTM-sub-regions; (6) LSTM-global; (7) Conv-SE-LSTM-sub-regions; and (8) Conv-SE-LSTM-global.

Table 7
Performance of the four models along the Sichuan-Tibet transportation corridor.

Zone	Models	Sub-region prediction results					Global prediction results				
		ACC	Precision	Recall	F-measure	AUC	ACC	Precision	Recall	F-measure	AUC
①	SVM	/	/	/	/	/	0.7275	0.7157	0.7547	0.7347	0.8033
	CNN	/	/	/	/	/	0.7537	0.7440	0.7736	0.7585	0.8381
	LSTM	/	/	/	/	/	0.7589	0.7906	0.7044	0.7450	0.8484
	Conv-SE-LSTM	/	/	/	/	/	0.8040	0.8085	0.7966	0.8025	0.8813
②	SVM	0.7431	0.7273	0.7778	0.7517	0.7963	0.7083	0.6471	0.9167	0.7586	0.7821
	CNN	0.7639	0.7375	0.8194	0.7763	0.8499	0.8160	0.7433	0.9653	0.8399	0.8992
	LSTM	0.7569	0.7569	0.7569	0.7569	0.8359	0.7882	0.7456	0.8750	0.8051	0.8504
	Conv-SE-LSTM	0.7674	0.7619	0.7778	0.7698	0.8371	0.8125	0.7473	0.9444	0.8344	0.8707
③	SVM	0.7447	0.7805	0.6809	0.7273	0.8352	0.6809	0.6491	0.7872	0.7115	0.8176
	CNN	0.9149	0.9333	0.8936	0.9130	0.9461	0.8830	0.8333	0.9574	0.8911	0.9715
	LSTM	0.8511	0.8667	0.8298	0.8478	0.9181	0.8404	0.8636	0.8085	0.8352	0.9208
	Conv-SE-LSTM	0.8936	0.9302	0.8511	0.8889	0.9579	0.8617	0.8400	0.8936	0.8660	0.9457
④	SVM	0.7294	0.7315	0.7248	0.7281	0.8209	0.6284	0.5972	0.7890	0.6798	0.7775
	CNN	0.7661	0.7458	0.8073	0.7753	0.8681	0.8440	0.8049	0.9083	0.8534	0.9156
	LSTM	0.7706	0.7921	0.7339	0.7619	0.8285	0.7890	0.8058	0.7615	0.7830	0.8615
	Conv-SE-LSTM	0.7982	0.8095	0.7798	0.7944	0.8755	0.8119	0.8208	0.7982	0.8093	0.8849
⑤	SVM	0.7629	0.7802	0.7320	0.7553	0.8444	0.7010	0.7600	0.5876	0.6628	0.7642
	CNN	0.8351	0.8155	0.8660	0.8400	0.9039	0.8814	0.9022	0.8557	0.8783	0.9463
	LSTM	0.7732	0.8118	0.7113	0.7582	0.8652	0.7629	0.8400	0.6495	0.7326	0.8943
	Conv-SE-LSTM	0.8196	0.7768	0.8969	0.8325	0.8971	0.8144	0.8280	0.7938	0.8105	0.8965
⑥	SVM	0.6707	0.6296	0.8293	0.7158	0.7827	0.7317	0.7714	0.6585	0.7105	0.8125
	CNN	0.7195	0.6800	0.8293	0.7473	0.8175	0.8720	0.8861	0.8537	0.8696	0.9304
	LSTM	0.7256	0.7033	0.7805	0.7399	0.8236	0.8171	0.8939	0.7195	0.7973	0.9210
	Conv-SE-LSTM	0.7561	0.7442	0.7805	0.7619	0.8294	0.8049	0.8906	0.6951	0.7808	0.9155

Notes: ① Global; ② Minjiang-Dadu River Basin; ③ Ya-lung River Basin; ④ Jinsha River Basin; ⑤ Salween-Lancang River Basin; and ⑥ Brahmaputra River Basin.

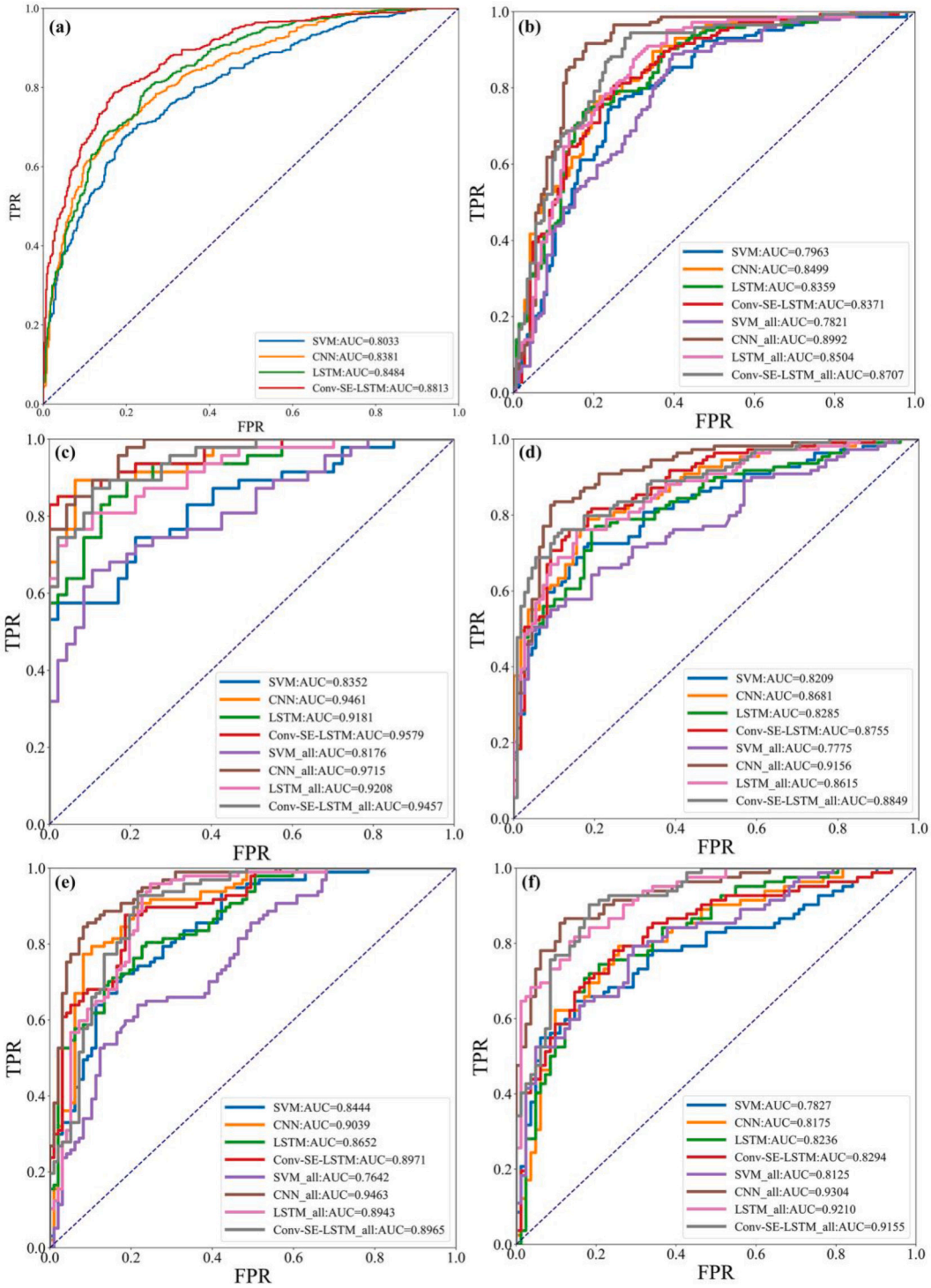

Fig. 14. ROC curves: (a) Global; (b) Minjiang-Dadu River Basin; (c) Ya-lung River Basin; (d) Jinsha River Basin; (e) Salween-Lancang River Basin; and (f) Brahmaputra River Basin.

5. Discussion

The geological environment along the Sichuan-Tibet transportation corridor is complex and landslides, along with other geological disasters, can occur easily (Cui et al., 2022). The occurrence of landslides is a very complicated process and controlled by several factors. LSM is of great significance for landslides prevention. In the present paper, the influence of the input sequences of different factor layers on the LSTM model is discussed, and a Conv-SE-LSTM model is also proposed based on the optimal sequence and applied to the LSM along the Sichuan-Tibet transportation corridor. Furthermore, the results of the model are compared with the traditional deep learning methods from global and sub-region perspectives. The results show that the model performance of the proposed method is far superior to that of the existing methods. In addition, the optimal Conv-SE-LSTM model was used to analyze changes in LSM under the influence of different dynamic factors in 2011 and 2016. What follows are the in-depth analysis of the robustness of the proposed model and the relationship between the change in landslide

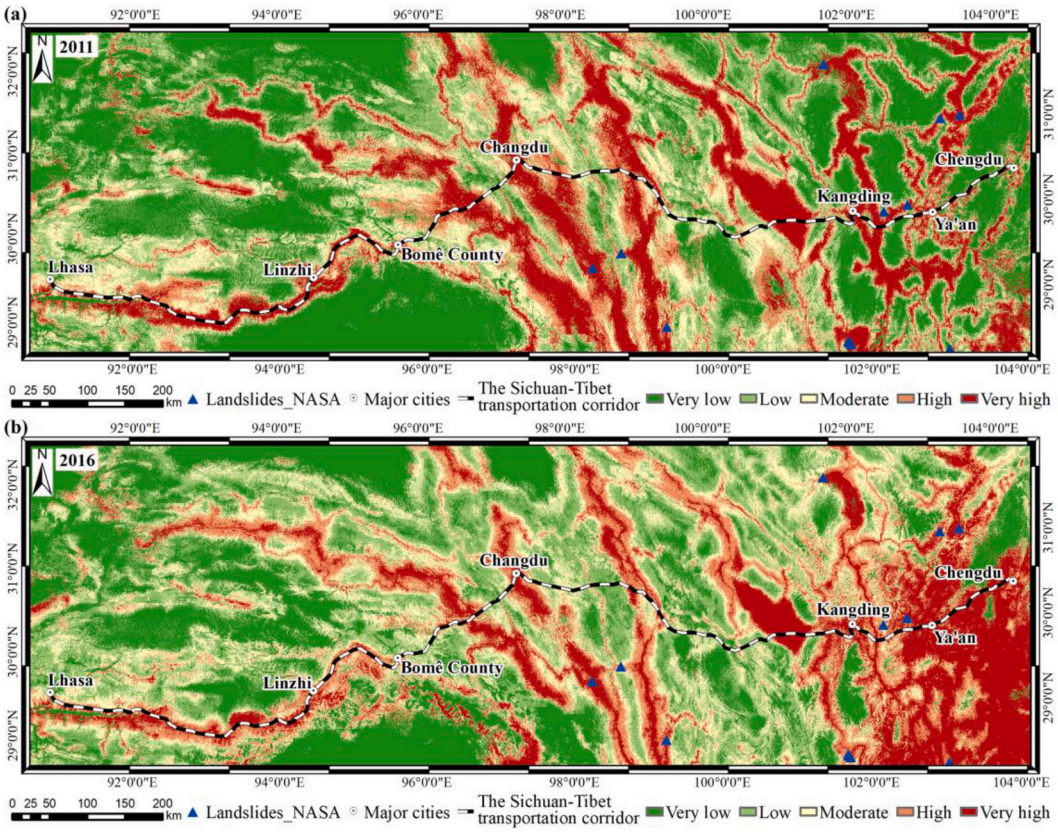

Fig. 15. Variation of the landslide susceptibility index under different NDVI and rainfall conditions: (a) 2011; and (b) 2016.

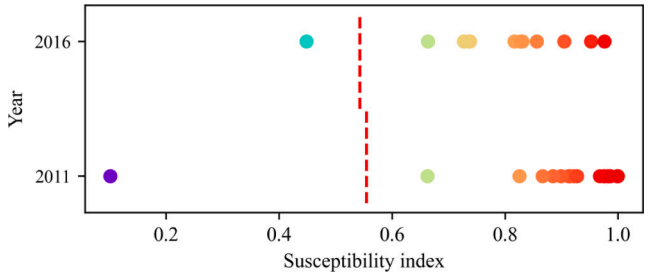

Fig. 16. Susceptibility index of landslide points predicted for 2011 and 2016.

susceptibility index and the dynamic factors.

5.1. How robust is the proposed Model?

Compared with the deep learning model, SVM model has shorter training time (Huang et al., 2022a), but its prediction performance was found to be the least reliable. CNN and LSTM are the two others commonly used deep learning algorithms (Wang et al., 2019; Wang et al., 2020). CNN can extract deep information from images, whereas LSTM can make full use of sequence information. Good results have been achieved using the above two methods in the study area. However, the performance of CNN is better than LSTM, which is consistent with the research conclusion of Thi Ngo et al. (2020). For LSM, the importance of different channels for the occurrence of landslides is different (Huang et al., 2022b), and the Conv–LSTM model considers that each channel of the feature map is equally important in the process of convolution and pooling (Wang et al., 2021). By introducing the SE attention module to construct the Conv-SE-LSTM model, the influence of applying different channels on model accuracy is solved. By processing the convoluted feature map, the SE module first obtains a one-dimensional vector of the same size as the number of channels, which is used as the weight of each channel. Then, the weight is applied to the corresponding channels to obtain the results. The experimental results show the AUC of the Conv-SE-LSTM model to be approximately 3 %, 4 % and 8 % higher than that obtained by three traditional methods, respectively. Since the Conv-SE-LSTM model displays a higher AUC value than the other three models, this implies that the proposed Conv-SE-LSTM has the best predictive performance. The SE module is easy to integrate, and only one module was added on the original basis, greatly improving the classification effect (Hu et al., 2020).

Using machine learning or deep learning to carry out landslide susceptibility assessment is essentially a binary classification problem, and the susceptibility index is the probability that the unit is divided into landslide. The higher the accuracy of the model, the closer the susceptibility index of landslide points is to 1, and the closer the susceptibility of non-landslide points is to 0, which leads to the relatively conservative of very high and high susceptibility areas in the LSMs. Compared with the LSM along the Sichuan-Tibet transportation corridor and its adjacent area using an improved frequency ratio method obtained by Li et al. (2017a), the distribution of very high and high susceptibility areas is relatively similar. They are distributed along the linear features such as water systems and roads in the study area and are mainly concentrated in several areas along the Dadu river, Jinsha river, Lancang river and Brahmaputra river. At the same time, the research results of Cui and Zou (2021) show that the sections with moderate susceptibility or above account for 70.43 % of the total length of the corridor, the high-risk sections account for 48.62 % of the total length of the corridor, and the risk-free sections account for 7.11 % of the total length of the corridor. Consistent with the previous classification criteria, the corresponding results in this research are 78.87 %, 48.63 % and 5.09 %, which are basically consistent. In addition, different from the traditional methods based on statistical models, the landslide susceptibility index obtained by machine learning or deep learning is always between 0 and

1 in any region, and the relative susceptibility of different regions cannot be reflected.

Previous studies rarely discussed the robustness of the model, section 4.4 presents the performance of the four models from different angles and different sub-regions. Fig. 17 shows the AUC values of different models for each sub-region from the global and sub-regions perspectives. The dark broken lines represent the results obtained from the global perspective and the light broken lines represent the results obtained from the sub-region perspective. It can be seen that the AUC values of the SVM model and LSTM model are relatively low, whereas the AUC values of the Conv-SE-LSTM and CNN models are higher. The average of the absolute difference values of the AUC of the SVM, CNN, LSTM and Conv-SE-LSTM models for each sub-region are 0.037, 0.056, 0.035 and 0.028, respectively. This demonstrates that the Conv-SE-LSTM model offers the greatest stability. Overall, the CNN model displays good performance but poor stability, the SVM and LSTM models show good stability but poor model performance, and the proposed Conv-SE-LSTM model offers the best stability and good robustness on the basis of the accuracy of LSM.

Comparing the Minjiang-Dadu River Basin, with its simple geological conditions and landslide disaster mechanism, with the Brahmaputra River basin, with its large area, few landslide points, complex geological conditions and simple sample information, there is a little difference in the AUC values and robustness of several of the deep learning models in terms of zoning and global prediction. The complex geological conditions and landslide disaster mechanisms in place for the Ya-lung River Basin, the Jinsha River Basin and the Salween-Lancang River Basin resulted in complex information within selected samples, low discrimination ability, poor feature extraction ability and poor model performance in the SVM model. The CNN and LSTM models were greatly affected by the number of samples and poor model stability. The proposed Conv-SE-LSTM model not only extracted the deep features of the samples fully, but also fully mined the information related to landslides occurrence. In this paper, the newly proposed model was systematically and detailly described from the perspectives of model construction, model training, model accuracy evaluation, statistical analysis of susceptibility results, and discussion of model robustness. The proposed Conv-SE-LSTM model was more stable in complex areas and large-range scenarios, and showed good prediction results. As a new deep learning model, it fully considers the conditions of each channel of input data for landslide susceptibility assessment, gives adaptive weights and makes full use of the sequence information between factors. From the perspective of model construction, it is more suitable for LSM work. However, there still need some improvement in how to improve the interpretability of the model and the relative degree of susceptibility between different regions. I hope to discuss and solve this problem with more scholars in the future.

5.2. *How does landslide susceptibility change with changes in various conditioning Factors?*

The deep learning model largely depends on the landslide training

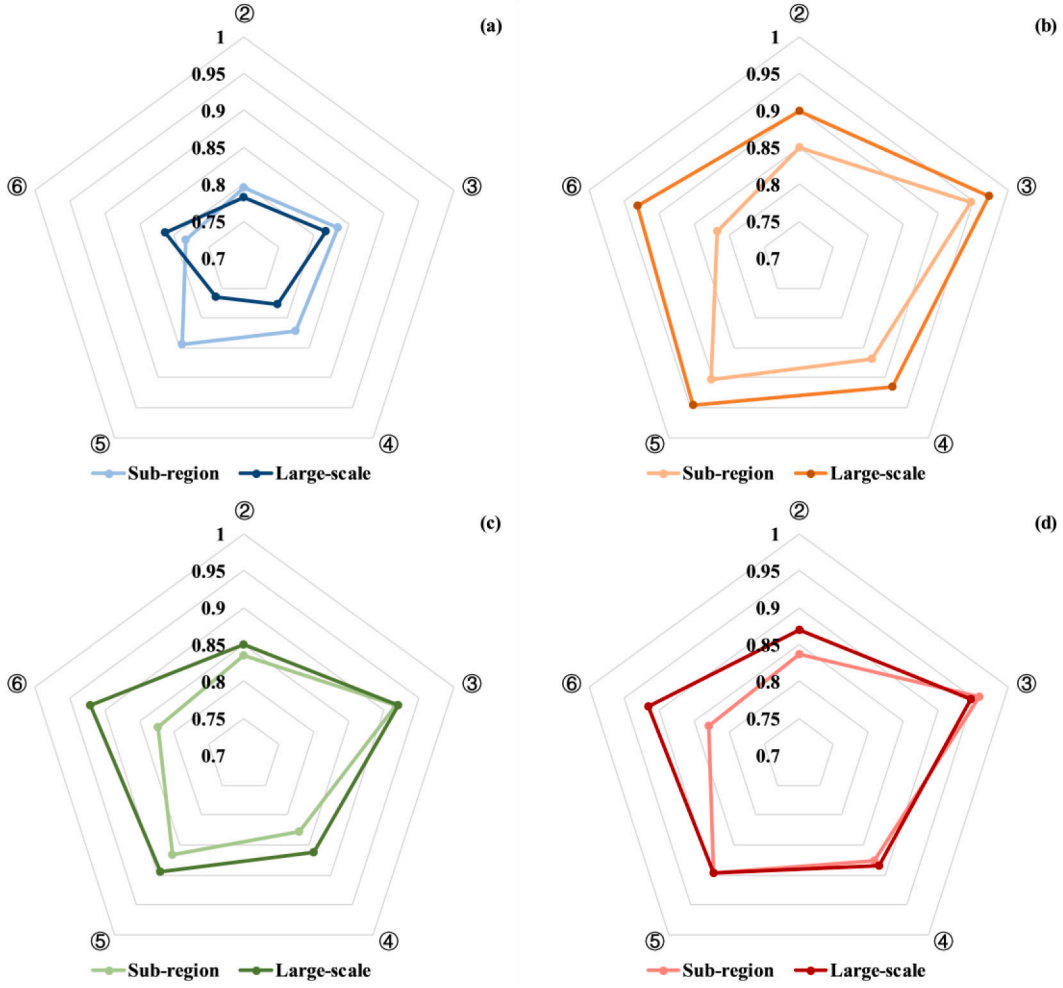

Fig. 17. Comparison of the robustness of different models: (a) SVM; (b) CNN; (c) LSTM; (d) Conv-SE-LSTM. Note: ② Minjiang-Dadu River Basin; ③ Ya-lung River Basin; ④ Jinsha River Basin; ⑤ Salween-Lancang River Basin; and ⑥ Brahmaputra River Basin.

samples. Fig. 18 summarizes the relationships between the landslides and each conditioning factor. The occurrence of landslides is affected by many factors. The statistical analysis of landslide distribution law in the present study area plays an important role in the selection of conditioning factors and the occurrence of landslides in the study area (Chen et al., 2022; Wu et al., 2020). Fig. 18 shows that, in the study area, altitudes in the range 4500 m-4900 m are highly prone to landslides. Landslides in the study area are mainly concentrated near slopes of 25° and 34°. Slopes that are too high or too low are not prone to landslides, and the aspect has no obvious distribution characteristics. The landslides are mostly distributed in the northeast, east and southwest. Also, curvatures that are too high or too low do not promote geological disasters, and the landslides are mostly concentrated within the curvature value –0.02–0.02, the plan curvature value 9–20, and the profile curvature value 4–12. The distribution of faults, rivers, roads and landslides follows a distribution law: the closer their distance, the greater the chance of landslide occurrence. Hard slate and quartz sandstone, hard granite, andesite and dolomite, soft and hard alternating metamorphic sandstone, marlite and phyllite promote the highest number of landslides. The landslides occur in areas with a surface roughness of 1–1.5, a relief amplitude of 15–60, a TWI value of 3.5–7. and in areas with rainfall of 477–780 mm/y, with a peak of 962 mm/y.

Among the conditioning factors selected in the research, rainfall and NDVI vary greatly with time, and have a greater impact on landslide occurrence. Therefore, it is significant to discuss the dynamic response relationship between dynamic factors (rainfall and NDVI) and landslide susceptibility (Hua et al., 2020). The annual scale landslide susceptibility prediction method based on deep learning proposed in the present paper is suitable for situations where fewer landslide data with accurate occurrence timing. Although the timescale in this study is yearly, the applicability of the model is more extensive, which provides new scope for the in-depth study of changes in susceptibility with time. The susceptibility maps of the study area for 2011 and 2016 obtained by the Conv-SE-LSTM model were verified by the Landslides_NASA, and the accuracy obtained for this method was 93.33 %.

Fig. 19(a) shows the variation of the landslide susceptibility index

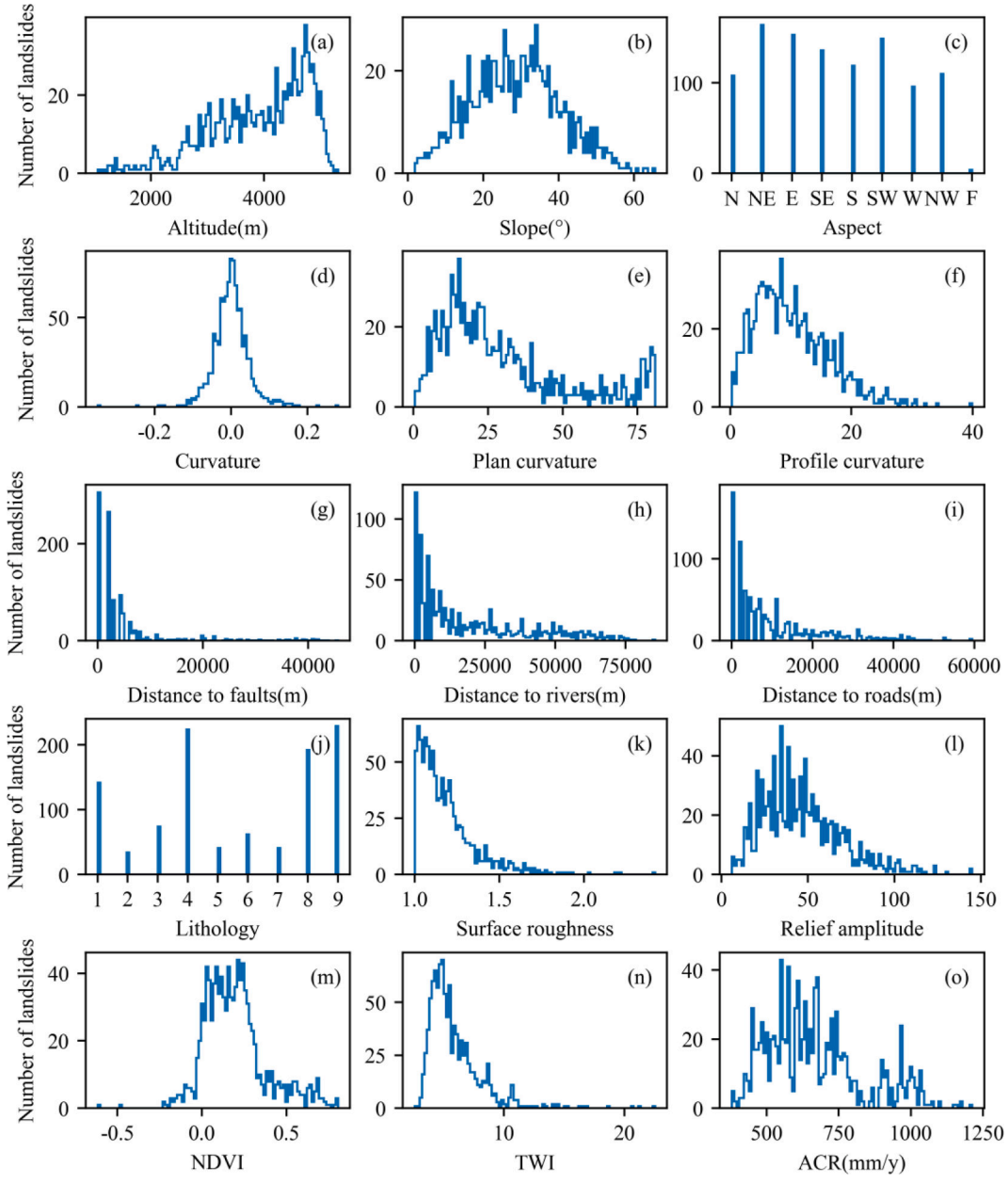

Fig. 18. Relationship between landslides and conditioning factors.

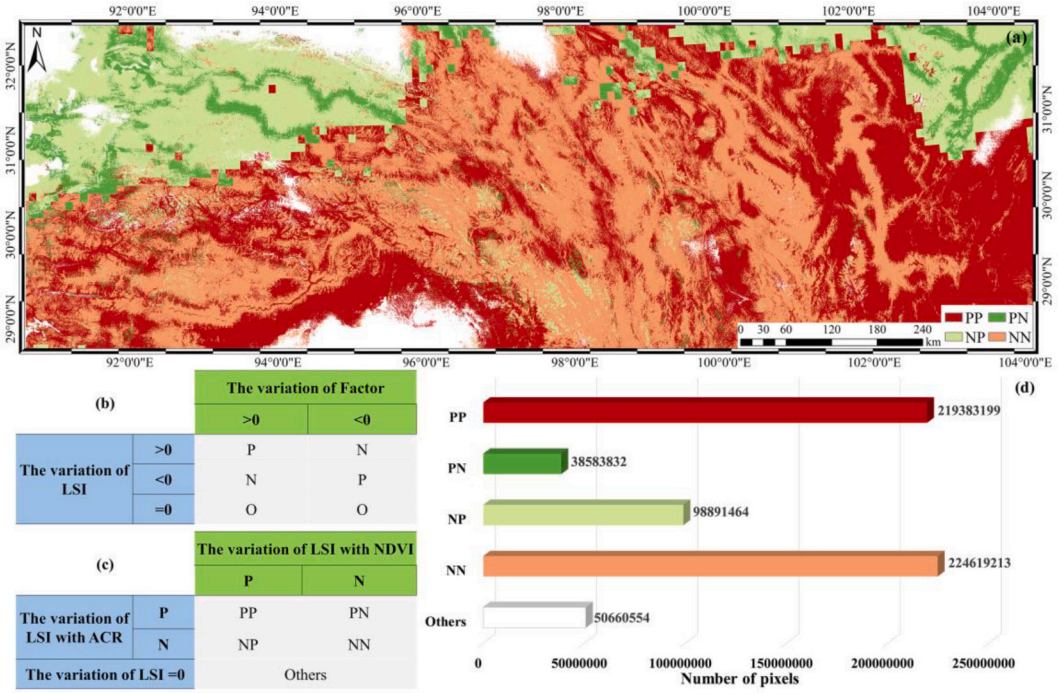

Fig. 19. The change analysis in LSI from 2011 to 2016: (a) variation of LSI with dynamic factors NDVI and ACR; (b) calculation method of the variation diagram of LSI with ACR or NDVI; (c) calculation method of the common variation diagram of LSI with ACR and NDVI and (d) statistical analysis of the common variation diagram of LSI with ACR and NDVI. P represents a positive correlation; N represents a negative correlation.

(LSI) with dynamic factors NDVI and ACR. First, the LSI change diagram, ACR change diagram and NDVI change diagram from 2011 to 2016 were calculated. Then, in accordance with the calculation method in Fig. 19 (b), the variation diagram of LSI with ACR and the variation diagram of LSI with NDVI were obtained. Finally, the common variation diagram of LSI with ACR and NDVI was obtained by the calculation method in Fig. 19(c). "PP" and "PN" represent the areas where the change in LSI positively related to rainfall. In these areas, rainfall erodes the slope surface, destroys the surface integrity of the rock and soil mass, reduces the shear strength of the rock and soil mass and, thus, increases the possibility of landslides (Li et al. 2017a; Ye et al., 2021). "PN" and "NN" indicate the areas where the change in LSI is negatively correlated with the NDVI value. The smaller the NDVI value, the lower the vegetation coverage, more unstable the water and soil conservation, and lower the shear strength of the slope (Wei et al., 2022; Guo et al., 2015). This increases the possibility of landslides occurrence. The white area indicates no change or little change (<0.01) in the susceptibility index between the two years.

The variation results of LSI with the dynamic factors NDVI and ACR were statistical and the results are shown in Fig. 19(d). According to the statistical results, the proportion of regions with a positive correlation between LSI change and rainfall or a negative correlation with NDVI value was 84.36 %, indicating that the LSI change in most of the regions is consistent with the actual situation. The annual scale change analysis method of landslide susceptibility based on deep learning proposed in this paper has certain reliability. From the statistical results, the positive correlation between the LSI change and rainfall accounted for only around 41 %, which was mainly concentrated in the Minjiang-Dadu River Basin and the Brahmaputra River Basin. This indicates a strong relationship between the occurrence of landslides and the dynamic response of rainfall in these two sub-regions. The negative correlation between the LSI change and NDVI accounted for about 42 %, and was mainly concentrated in the Ya-lung River Basin, the Jinsha River Basin and the Salween-Lancang River Basin, indicating that the occurrence of landslides has a strong relationship with the dynamic response of NDVI and is less affected by rainfall. In some areas (white, about 0.08 %), the LSI index in 2011 was very high (close to 1) or very low (close to 0). Furthermore, for 2016, although the ACR increased or NDVI decreased, the LSI value remained unchanged or changed only slightly. This can be related to the "*softmax*" activation function used by the deep learning method in the final classification layer. After the extracted effective features passed through the *softmax* layer, the landslide probability value between 0 and 1 was obtained. Therefore, for all practical applications, it is necessary to pay attention not only to the areas where the LSI index increase, but also to the high and very high susceptibility areas after prediction.

The occurrence of landslides is affected by many factors. In the landslide susceptibility dynamic assessment for a wide range, only rainfall and NDVI are considered according to the availability and accessibility of data. In future work, we will further optimize and adjust to explore the dynamic response relationship between other factors (such as human engineering activities) and landslide occurrence.

6. Conclusions

In the present study, the effects of input sequences of different factor layers on the accuracy of the LSTM model were compared. It was proved that the input factor sequence based on decreasing IGR values can make full use of the sequence information of the factors and show better performance. Secondly, a Conv-SE-LSTM model was proposed which introduced the SE attention mechanism into the deep learning method and mapped landslide susceptibility along the Sichuan-Tibet transportation corridor. It was found that the AUC of the proposed Conv-SE-LSTM model was approximately 3 %, 4 % and 8 % higher than that of the CNN model, LSTM model and SVM model, respectively. This verified that the Conv-SE-LSTM algorithms exhibited excellent performance and capability in assessing landslide susceptibility along the Sichuan-Tibet transportation corridor in China.

According to different geological environments, the study area was divided into five sub-regions, and the landslide susceptibility evaluation was carried out within those sub-regions. The results showed that global prediction was more accurately forecast by the CNN, LSTM and Conv-

SE-LSTM models, whereas sub-region prediction was better forecast by the SVM model. The performance of the proposed Conv-SE-LSTM model was less affected by the environment and sample size than the other models, and offered stronger feature extraction ability and greater robustness. Finally, based on the optimal Conv–SE-LSTM model under MYACR and NDVI-mean conditions, the landslide susceptibility maps of the study area for 2011 and 2016 were obtained. The actual occurrence time of the landslides were used for verification, and the results obtained through this method matched with the reality with an accuracy rate of 93.33 %. The statistical analysis of susceptibility changes from 2011 to 2016 show the method proposed in this paper based on deep learning on an annual scale to offer certain reliability.

Declaration of Competing Interest

The authors declare that they have no known competing financial interests or personal relationships that could have appeared to influence the work reported in this paper.

Data availability

Data will be made available on request.

Acknowledgements

This work was funded by the National Key Research and Development Program of China (Grant No. 2021YFC3000400). Part of this work was also funded by the National Natural Science Foundation of China (Grant Nos. 41941019, 42090053, 42041006), the Shaanxi Province Science and Technology Innovation team (Grant No. 2021TD-51), the Shaanxi Province Geoscience Big Data and Geohazard Prevention Innovation Team (2022), the Fundamental Research Funds for the Central Universities, CHD (Grant Nos. 300102260301, 300102261108, 300102262902, 300102269208, 300102260404), and the Fund Project of Shaanxi Key Laboratory of Land Consolidation (Grant No. 2019-ZD04). The authors are grateful to the editor of the journal and the anonymous reviewers for their valuable comments and recommendations. Thanks to Chang'an University High Performance Computing Platform.

References

Aditian, A., Kubota, T., Shinohara, Y., 2018. Comparison of GIS-based landslide susceptibility models using frequency ratio, logistic regression, and artificial neural network in a tertiary region of Ambon, Indonesia. Geomorphology 318, 101–111. https://doi.org/10.1016/j.geomorph.2018.06.006.

Al-Najjar, H.A.H., Pradhan, B., 2021. Spatial landslide susceptibility assessment using machine learning techniques assisted by additional data created with generative adversarial networks. Geosci. Front. 12, 625–637. https://doi.org/10.1016/j.gsf.2020.09.002.

Awad, M., Khanna, R., 2015. Support Vector Machines for Classification, Efficient Learning Machines: Theories, Concepts, and Applications for Engineers and System Designers. Apress, Berkeley, CA, pp. 39–66.

Bathrellos, G.D., Skilodimou, H.D., Chousianitis, K., Youssef, A.M., Pradhan, B., 2017. Suitability estimation for urban development using multi-hazard assessment map. Sci Total Environ 575, 119–134. https://doi.org/10.1016/j.scitotenv.2016.10.025.

Caine, N., 1980. The Rainfall Intensity: Duration Control of Shallow Landslides and Debris Flows. Geografiska Annaler. Series A, Physical Geography 62, 23–27. https://doi.org/10.2307/520449.

Can, R., Kocaman, S., Gokceoglu, C., 2019. A Convolutional Neural Network Architecture for Auto-Detection of Landslide Photographs to Assess Citizen Science and Volunteered Geographic Information Data Quality. ISPRS Int. J. Geo Inf. 8, 300. https://doi.org/10.3390/ijgi8070300.

Chen, B., Li, Z., Zhang, C., Ding, M., Zhu, W., Zhang, S., Han, B., Du, J., Cao, Y., Zhang, C., Liao, Z., Zhou, S., Wang, J., Peng, J., 2022. Wide Area Detection and Distribution Characteristics of Landslides along Sichuan Expressways. Remote Sens. (Basel) 2022 (14), 3431. https://doi.org/10.3390/rs14143431.

Chen, W., Zhang, S., Li, R., Shahabi, H., 2018. Performance evaluation of the GIS-based data mining techniques of best-first decision tree, random forest, and naive Bayes tree for landslide susceptibility modeling. Sci Total Environ 644, 1006–1018. https://doi.org/10.1016/j.scitotenv.2018.06.389.

Cui, P., Ge, Y., Li, S., Li, Z., Xu, X., Zhou, G.G.D., Chen, H., Wang, H., Lei, Y., Zhou, L., Yi, S., Wu, C., Guo, J., Wang, Q., Lan, H., Ding, M., Ren, J., Zeng, L., Jiang, Y., Wang, Y., 2022. Scientific Challenges in Disaster Risk Reduction for the Sichuan-Tibet Railway. Eng. Geol. 309 https://doi.org/10.1016/j.enggeo.2022.106837.

Cui, P., Zou, Q., 2021. Evolution law and engineering risk of mountain hazards in Sichuan-Tibet traffic corridor. Science Press, Beijing, p. 432. In Chinese.

Dao, D.V., Jaafari, A., Bayat, M., Mafi-Gholami, D., Qi, C., Moayedi, H., Phong, T.V., Ly, H.B., Le, T.T., Trinh, P.T., Luu, C., Quoc, N.K., Thanh, B.N., Pham, B.T., 2020. A spatially explicit deep learning neural network model for the prediction of landslide susceptibility. Catena 188, 104451. https://doi.org/10.1016/j.catena.2019.104451.

Dash, M., Liu, H., 1997. Feature selection for classification. Intell. Data Anal. 1, 131–156. https://doi.org/10.1016/S1088-467X(97)00008-5.

Di Napoli, M., Carotenuto, F., Cevasco, A., Confuorto, P., Di Martire, D., Firpo, M., Pepe, G., Raso, E., Calcaterra, D., 2020. Machine learning ensemble modelling as a tool to improve landslide susceptibility mapping reliability. Landslides 17, 1897–1914. https://doi.org/10.1007/s10346-020-01392-9.

Ermini, L., Catani, F., Casagli, N., 2005. Artificial Neural Networks applied to landslide susceptibility assessment. Geomorphology 66, 327–343. https://doi.org/10.1016/j.geomorph.2004.09.025.

Fang, Z., Wang, Y., Peng, L., Hong, H., 2020. Integration of convolutional neural network and conventional machine learning classifiers for landslide susceptibility mapping. Comput. Geosci. 139, 104470 https://doi.org/10.1016/j.cageo.2020.104470.

Goyes-Peñafiel, P., Hernandez-Rojas, A., 2021. Landslide susceptibility index based on the integration of logistic regression and weights of evidence: A case study in Popayan. Colombia. Engineering Geology 280, 105958. https://doi.org/10.1016/j.enggeo.2020.105958.

Graves, A., 2012. Supervised Sequence Labelling with Recurrent Neural Networks. Studies in Computational Intelligence 385. https://doi.org/10.1007/978-3-642-24797-2.

Guo, C., Zhang, Y., Jiang, L., Shi, J., Meng, W., Du, Y., Ma, C., 2017. Discussion on the Environmental and Engineering Geological Problems Along the Sichuan-Tibet Railway and Its Adjacent Area. Geoscience, 31, 877-889. https://doi.org/j.issn.1000-8527.2017.05.001. (In Chinese).

Guo, C., Montgomery, D.R., Zhang, Y., Wang, K., Yang, Z., 2015. Quantitative assessment of landslide susceptibility along the Xianshuihe fault zone, Tibetan Plateau, China. Geomorphology 248, 93–110. https://doi.org/10.1016/j.geomorph.2015.07.012.

Hanley, J.A., McNeil, B.J., 1982. The meaning and use of the area under a receiver operating characteristic (ROC) curve. Radiology 143, 29–36. https://doi.org/10.1148/radiology.143.1.7063747.

Hochreiter, S., Schmidhuber, J., 1997. Long Short-Term Memory. Neural Comput. 9, 1735–1780. https://doi.org/10.1162/neco.1997.9.8.1735.

Hou, X., Bai, Y., Li, Y., Shang, C., Shen, Q., 2021. High-resolution triplet network with dynamic multiscale feature for change detection on satellite images. ISPRS J. Photogramm. Remote Sens. 177, 103–115. https://doi.org/10.1016/j.isprsjprs.2021.05.001.

Hu, J., Shen, L., Albanie, S., Sun, G., Wu, E.H., 2020. Squeeze-and-Excitation Networks. IEEE Trans. Pattern Anal. Mach. Intell. 42, 2011–2023. https://doi.org/10.1109/tpami.2019.2913372.

Hua, Y., Wang, X., Li, Y., Xu, P., Xia, W., 2020. Dynamic Development of Landslide Susceptibility Based on Slope Unit and Deep Neural Networks. Landslides 18 (1), 281–302. https://doi.org/10.1007/s10346-020-01444-0.

Huang, W.B., Ding, M.T., Li, Z.H., Zhuang, J.Q., Yang, J., Li, X.L., Meng, L.E., Zhang, H. Y., Dong, Y., 2022a. An Efficient User-Friendly Integration Tool for Landslide Susceptibility Mapping Based on Support Vector Machines: SVM-LSM Toolbox. Remote Sens. (Basel) 14, 3408. https://doi.org/10.3390/rs14143408.

Huang, W.B., Ding, M.T., Wang, D., Jiang, L.W., Li, Z.H., 2022b. Evaluation of Landslide Susceptibility Based on Layer Adaptive Weighted Convolutional Neural Network Model along Sichuan-Tibet Traffic Corridor. Earth Sci. 47 (6), 2015–2030. In Chinese.

Ji, S., Yu, D., Shen, C., Li, W., Xu, Q., 2020. Landslide detection from an open satellite imagery and digital elevation model dataset using attention boosted convolutional neural networks. Landslides 17, 1337–1352. https://doi.org/10.1007/s10346-020-01353-2.

Jones, J.N., Boulton, S.J., Bennett, G.L., Stokes, M., Whitworth, M.R.Z., 2021. Temporal Variations in Landslide Distributions Following Extreme Events: Implications for Landslide Susceptibility Modeling. J. Geophys. Res. Earth 126. https://doi.org/10.1029/2021jf006067.

Karakas, G., Kocaman, S., Gokceoglu, C., 2022. Comprehensive performance assessment of landslide susceptibility mapping with MLP and random forest: a case study after Elazig earthquake (24 Jan 2020, Mw 6.8), Turkey. Environmental Earth Sciences, 81, 144. https://doi.org/10.1007/s12665-022-10225-y.

Kocaman, S., Tavus, B., Nefeslioglu, H.A., Karakas, G., Gokceoglu, C., Sarihan, N.H., 2020. Evaluation of Floods and Landslides Triggered by a Meteorological Catastrophe (Ordu, Turkey, August 2018) Using Optical and Radar Data. Geofluids 2020, 1–18. https://doi.org/10.1155/2020/8830661.

Kritikos, T., Davies, T., 2014. Assessment of rainfall-generated shallow landslide/debris-flow susceptibility and runout using a GIS-based approach: application to western Southern Alps of New Zealand. Landslides 12, 1051–1075. https://doi.org/10.1007/s10346-014-0533-6.

Krizhevsky, A., Sutskever, I., Hinton, G.E., 2017. ImageNet classification with deep convolutional neural networks. Commun. ACM 60, 84–90. https://doi.org/10.1145/3065386.

Lee, S., Baek, W.K., Jung, H.S., Lee, S., 2020. Susceptibility Mapping on Urban Landslides Using Deep Learning Approaches in Mt. Umyeon. Applied Sciences 10, 8189. https://doi.org/10.3390/app10228189.

Li, L., Lan, H., Guo, C., Zhang, Y., Li, Q., Wu, Y., 2017a. Geohazard Susceptibility Assessment Along the Sichuan-Tibet Railway and Its Adjacent Area Using an

Improved Frequency Ratio Method. Geoscience 31, 911–929. https://doi.org/10.3969/j.issn.1000-8527.2017.05.004. (In Chinese).
Li, L., Lan, H., Guo, C., Zhang, Y., Li, Q., Wu, Y., 2017b. A modified frequency ratio method for landslide susceptibility assessment. Landslides 14, 727–741. https://doi.org/10.1007/s10346-016-0771-x.
Li, Y., Wang, X., Mao, H., 2020. Influence of Human Activity on Landslide Susceptibility Development in the Three Gorges Area. Nat. Hazards 104, 2115–2151. https://doi.org/10.1007/s11069-020-04264-6.
Li, Z.H., Zhang, C.L., Chen, B., Zhan, J.W., Ding, M.T., Lv, Y., Li, X.L., Peng, J.B., 2022. A Technical Framework of Landslide Prevention Based on Multi-Source Remote Sensing and Its Engineering Application. Earth Sci. 47 (6), 1901–1916. In Chinese.
Lyu, H.M., Shen, J., Arulrajah, A., 2018. Assessment of Geohazards and Preventative Countermeasures Using AHP Incorporated with GIS in Lanzhou, China. Sustainability 10, 304–325. https://doi.org/10.3390/su10020304.
Mohan, A., Singh, A.K., Kumar, B., Dwivedi, R., 2021. Review on remote sensing methods for landslide detection using machine and deep learning. Trans. Emerg. Telecommun. Technol. 32, 23. https://doi.org/10.1002/ett.3998.
Mutlu, B., Nefeslioglu, H.A., Sezer, E.A., Akcayol, M.A., Gokceoglu, C., 2019. An Experimental Research on the Use of Recurrent Neural Networks in Landslide Susceptibility Mapping. ISPRS Int. J. Geo Inf. 8, 21. https://doi.org/10.3390/ijgi8120578.
Nefeslioglu, H.A., Sezer, E.A., Gokceoglu, C., Ayas, Z., 2013. A modified analytical hierarchy process (M-AHP) approach for decision support systems in natural hazard assessments. Comput. Geosci. 59, 1–8. https://doi.org/10.1016/j.cageo.2013.05.010.
Peng, J., Cui, P., Zhuang, J., 2020. Challenges to engineering geology of Sichuan-Tibet railway. Chinese Journal of Rock Mechanics and Engineering, 39, 2377-2389. https://doi.org/10.13722/j.cnki.jrme.2020.0446. (In Chinese).
Pradhan, B., 2013. A comparative study on the predictive ability of the decision tree, support vector machine and neuro-fuzzy models in landslide susceptibility mapping using GIS. Comput. Geosci. 51, 350–365. https://doi.org/10.1016/j.cageo.2012.08.023.
Pradhan, A.M.S., Lee, S.R., Kim, Y.T., 2018. A Shallow Slide Prediction Model Combining Rainfall Threshold Warnings and Shallow Slide Susceptibility in Busan, Korea. Landslides 16, 647–659. https://doi.org/10.1007/s10346-018-1112-z.
Qi, T., Zhao, Y., Meng, X., Chen, G., Dijkstra, T., 2021. AI-Based Susceptibility Analysis of Shallow Landslides Induced by Heavy Rainfall in Tianshui. China. Remote Sensing 13, 1819. https://doi.org/10.3390/rs13091819.
Rabby, Y.W., Ishtiaque, A., Rahman, M.S., 2020. Evaluating the Effects of Digital Elevation Models in Landslide Susceptibility Mapping in Rangamati District. Bangladesh. Remote Sensing 12, 2718. https://doi.org/10.3390/rs12172718.
Regmi, N.R., Giardino, J.R., McDonald, E.V., Vitek, J.D., 2013. A comparison of logistic regression-based models of susceptibility to landslides in western Colorado, USA. Landslides 11, 247–262. https://doi.org/10.1007/s10346-012-0380-2.
Reichenbach, P., Rossi, M., Malamud, B.D., Mihir, M., Guzzetti, F., 2018. A review of statistically-based landslide susceptibility models. Earth Sci. Rev. 180, 60–91. https://doi.org/10.1016/j.earscirev.2018.03.001.
Sameen, M.I., Pradhan, B., Lee, S., 2020. Application of convolutional neural networks featuring Bayesian optimization for landslide susceptibility assessment. Catena 186, 104249. https://doi.org/10.1016/j.catena.2019.104249.
Shi, X.J., Chen, Z.R., Wang, H., Yeung, D.Y., Wong, W.K., Woo, W.C., 2015. Convolutional LSTM Network: A Machine Learning Approach for Precipitation Nowcasting. In: Cortes, C., Lawrence, N.D., Lee, D.D., Sugiyama, M., Garnett, R. (Eds.), Advances in Neural Information Processing Systems 28. Neural Information Processing Systems (Nips), La Jolla.
Sun, D., Wen, H., Wang, D., Xu, J., 2020. A random forest model of landslide susceptibility mapping based on hyperparameter optimization using Bayes algorithm. Geomorphology 362, 107201. https://doi.org/10.1016/j.geomorph.2020.107201.
Sun, D., Xu, J., Wen, H., Wang, D., 2021. Assessment of landslide susceptibility mapping based on Bayesian hyperparameter optimization: A comparison between logistic regression and random forest. Eng. Geol. 281, 105972 https://doi.org/10.1016/j.enggeo.2020.105972.
Tien Bui, D., Ho, T.C., Pradhan, B., Pham, B.T., Nhu, V.H., Revhaug, I., 2016. GIS-based modeling of rainfall-induced landslides using data mining-based functional trees classifier with AdaBoost, Bagging, and MultiBoost ensemble frameworks. Environ. Earth Sci. 75, 1101–1123. https://doi.org/10.1007/s12665-016-5919-4.
Torizin, J., Wang, L.C., Fuchs, M., Tong, B., Balzer, D., Wan, L.Q., Kuhn, D., Li, A., Chen, L., 2018. Statistical Landslide Susceptibility Assessment in a Dynamic Environment: A Case Study for Lanzhou City, Gansu Province, Nw China. J. Mt. Sci. 15, 1299–1318. https://doi.org/10.1007/s11629-017-4717-0.
Wang, Y., Fang, Z., Hong, H., 2019. Comparison of convolutional neural networks for landslide susceptibility mapping in Yanshan County, China. Sci Total Environ 666, 975–993. https://doi.org/10.1016/j.scitotenv.2019.02.263.
Wang, Y., Fang, Z., Wang, M., Peng, L., Hong, H., 2020. Comparative study of landslide susceptibility mapping with different recurrent neural networks. Comput. Geosci. 138, 104445 https://doi.org/10.1016/j.cageo.2020.104445.
Wang, H., Zhang, L., Luo, H., He, J., Cheung, R.W.M., 2021. AI-powered landslide susceptibility assessment in Hong Kong. Eng. Geol. 288, 106103 https://doi.org/10.1016/j.enggeo.2021.106103.
Wei, R., Ye, C., Ge, Y., Li, Y., 2022. An attention-constrained neural network with overall cognition for landslide spatial prediction. Landslides 19, 1087–1099. https://doi.org/10.1007/s10346-021-01841-z.
Wu, R., Zhang, Y., Guo, C., Yang, Z., Tang, J., Su, F., 2020. Landslide susceptibility assessment in mountainous area: a case study of Sichuan-Tibet railway. China. Environmental Earth Sciences 79. https://doi.org/10.1007/s12665-020-8878-8.
Xu, C., Dai, F., Xu, X., Lee, Y.H., 2012. GIS-based support vector machine modeling of earthquake-triggered landslide susceptibility in the Jianjiang River watershed, China. Geomorphology 145–146, 70–80. https://doi.org/10.1016/j.geomorph.2011.12.040.
Yang, X., Liu, R., Yang, M., Chen, J., Liu, T., Yang, Y., Chen, W., Wang, Y., 2021. Incorporating Landslide Spatial Information and Correlated Features among Conditioning Factors for Landslide Susceptibility Mapping. Remote Sens. (Basel) 13, 2166–2190. https://doi.org/10.3390/rs13112166.
Yao, J., Qin, S., Qiao, S., Che, W., Chen, Y., Su, G., Miao, Q., 2020. Assessment of Landslide Susceptibility Combining Deep Learning with Semi-Supervised Learning in Jiaohe County, Jilin Province, China. Appl. Sci. 10, 5640–5664. https://doi.org/10.3390/app10165640.
Ye, C.M., Wei, R.L., Ge, Y.G., Li, Y., Junior, J.M., Li, J., 2021. Gis-Based Spatial Prediction of Landslide Using Road Factors and Random Forest for Sichuan-Tibet Highway. J. Mt. Sci. 19, 461–476. https://doi.org/10.1007/s11629-021-6848-6.
Yi, Y., Zhang, Z., Zhang, W., Jia, H., Zhang, J., 2020. Landslide susceptibility mapping using multiscale sampling strategy and convolutional neural network: A case study in Jiuzhaigou region. Catena 195, 104851. https://doi.org/10.1016/j.catena.2020.104851.
Yu, L., Cao, Y., Zhou, C., Wang, Y., Huo, Z., 2019. Landslide Susceptibility Mapping Combining Information Gain Ratio and Support Vector Machines: A Case Study from Wushan Segment in the Three Gorges Reservoir Area, China. Appl. Sci. 9, 4756–4775. https://doi.org/10.3390/app9224756.
Zeng, B., Chen, X., 2021. Assessment of shallow landslide susceptibility using an artificial neural network. Arab. J. Geosci. 14, 499. https://doi.org/10.1007/s12517-021-06843-8.
Zhang, Y.X., Lan, H.X., Li, L.P., Wu, Y.M., Chen, J.H., Tian, N.M., 2020. Optimizing the frequency ratio method for landslide susceptibility assessment: A case study of the Caiyuan Basin in the southeast mountainous area of China. J. Mt. Sci. 17, 340–357. https://doi.org/10.1007/s11629-019-5702-6.